Weerasinghe-Mudiyanselage et al. *Zool. Res.* 2024, 45(2): 398−414
https://doi.org/10.24272/j.issn.2095-8137.2023.309

ZR | Zoological Research

Article Open Access

Changes in structural plasticity of hippocampal neurons in an animal model of multiple sclerosis

Poornima D.E. Weerasinghe-Mudiyanselage[1,#], Sohi Kang[1,2,#], Joong-Sun Kim[1], Sung-Ho Kim[1], Hongbing Wang[3], Taekyun Shin[4], Changjong Moon[1,*]

[1] *Department of Veterinary Anatomy and Animal Behavior*, *College of Veterinary Medicine and BK21 FOUR Program*, *Chonnam National University*, *Gwangju* 61186, *Republic of Korea*

[2] *Department of Anatomy and Convergence Medical Science*, *Institute of Health Sciences*, *College of Medicine*, *Gyeongsang National University*, *Jinju* 52727, *Republic of Korea*

[3] *Department of Physiology and Neuroscience Program*, *Michigan State University*, *East Lansing*, *MI* 48824, *USA*

[4] *Department of Veterinary Anatomy*, *College of Veterinary Medicine and Veterinary Medical Research Institute*, *Jeju National University*, *Jeju* 63243, *Republic of Korea*

ABSTRACT

Structural plasticity is critical for the functional diversity of neurons in the brain. Experimental autoimmune encephalomyelitis (EAE) is the most commonly used model for multiple sclerosis (MS), successfully mimicking its key pathological features (inflammation, demyelination, axonal loss, and gliosis) and clinical symptoms (motor and non-motor dysfunctions). Recent studies have demonstrated the importance of synaptic plasticity in EAE pathogenesis. In the present study, we investigated the features of behavioral alteration and hippocampal structural plasticity in EAE-affected mice in the early phase (11 days post-immunization, DPI) and chronic phase (28 DPI). EAE-affected mice exhibited hippocampus-related behavioral dysfunction in the open field test during both early and chronic phases. Dendritic complexity was largely affected in the cornu ammonis 1 (CA1) and CA3 apical and dentate gyrus (DG) subregions of the hippocampus during the chronic phase, while this effect was only noted in the CA1 apical subregion in the early phase. Moreover, dendritic spine density was reduced in the hippocampal CA1 and CA3 apical/basal and DG subregions in the early phase of EAE, but only reduced in the DG subregion during the chronic phase. Furthermore, mRNA levels of proinflammatory cytokines (*Il1β*, *Tnfα*, and *Ifnγ*) and glial cell markers (*Gfap* and *Cd68*) were significantly increased, whereas the expression of activity-regulated cytoskeleton-associated protein (ARC) was reduced during the chronic phase. Similarly, exposure to the aforementioned cytokines in primary cultures of hippocampal neurons reduced dendritic complexity and ARC expression. Primary cultures of hippocampal neurons also showed significantly reduced extracellular signal-regulated kinase (ERK) phosphorylation upon treatment with proinflammatory cytokines. Collectively, these results suggest that autoimmune neuroinflammation alters structural plasticity in the hippocampus, possibly through the ERK-ARC pathway, indicating that this alteration may be associated with hippocampal dysfunctions in EAE.

Keywords: Activity-regulated cytoskeleton-associated protein; Anxiety-like behavior; Experimental autoimmune encephalomyelitis; Hippocampal dysfunction; Neuroinflammation

INTRODUCTION

Multiple sclerosis (MS) is an autoimmune inflammatory disease of the central nervous system (CNS). The pathogenesis of MS involves an attack by the immune system against myelin sheath antigens, resulting in pathological motor deficits (Sloane et al., 2009). Many MS patients also experience hippocampus-related non-motor symptoms, such as memory impairment and depression (Brochet & Ruet, 2019; Rocca et al., 2018; Rouleau et al., 2018; Weerasinghe-Mudiyanselage et al., 2024). Hippocampal involvement in MS is further strengthened by extensive demyelination (Geurts et al., 2007), neuronal loss (Carassiti et al., 2018), and synaptic abnormalities (Dutta et al., 2011) in this brain region. Accumulating evidence suggests a direct link between neuroinflammation and synaptic abnormalities in the

Received: 04 December 2023; Accepted: 25 December 2023; Online: 26 December 2023

Foundation items: This study was supported by the National Research Foundation (NRF) of Korea Grant funded by the Korean Government (NRF-2022R1A2C100402212; RS-2023-00219517)

#Authors contributed equally to this work

*Corresponding author, E-mail: moonc@chonnam.ac.kr

hippocampi of patients with MS (Gentile et al., 2015; Michailidou et al., 2015). Inflammatory cytokines and neurotrophins released by immune cells alter synaptic plasticity (Stampanoni Bassi et al., 2022, 2019), related to the cognitive deficits observed in MS patients (Di Filippo et al., 2018; Stampanoni Bassi et al., 2017). Thus, hippocampal neuroinflammation and synaptic abnormalities have gained attention as plausible mechanisms underlying the cognitive and emotional impairments observed in MS sufferers (Colasanti et al., 2016; Rocca et al., 2018).

Experimental autoimmune encephalomyelitis (EAE) is a commonly employed animal model for investigating MS due to its capacity to replicate primary histopathological characteristics, such as inflammation, demyelination, axonal loss, and gliosis, as well as clinical manifestations, encompassing both motor and non-motor symptoms (Furlan et al., 2009; Hong et al., 2023; Procaccini et al., 2015). Within the context of EAE, cognitive impairments have been consistently reported across various phases of the disease. A growing body of evidence suggests that immune molecules and neuroinflammation impact synaptic plasticity, a fundamental mechanism underlying cognitive function (Di Filippo et al., 2008). During EAE progression, significant alterations in synaptic plasticity have been observed in the hippocampus, an essential neuronal structure implicated in cognitive processes (Di Filippo et al., 2015; Novkovic et al., 2015). Synaptic dysfunction in the hippocampal cornu ammonis (CA) 1 subregion of mice with EAE has been observed at two different time points post-immunization (PI): 13–16 days and 25–35 days, corresponding to the onset (early) (Tu et al., 2009; Ziehn et al., 2010) and recovery/remitting (chronic) phases (Di Filippo et al., 2016; Novkovic et al., 2015), respectively. Clinical symptoms in mice typically manifest between 10–13 days post-immunization (DPI), ranging from a flaccid tail to limb paralysis. After this acute phase, mice enter a remission/chronic stage, regaining motor function to some extent by 18 DPI (Khorshid Ahmad et al., 2017). In the current study, we designated 11 DPI as the acute phase, signifying the onset of clinical symptoms, and 28 DPI as the chronic phase, representing the period during which mice sustain a chronic/persistent clinical score.

The EAE animal model also recapitulates varying degrees of cognitive and emotional dysregulation at these time points (Acharjee et al., 2013; Dutra et al., 2013; Kim et al., 2012). Although most researchers propose synaptic dysfunction as the underpinning mechanism for behavioral alterations observed in animal models of MS, the entire mechanism is still unclear. In our previous study, we observed a significant down-regulation in neuronal plasticity-associated and learning/memory-associated gene sets in the hippocampi of EAE mice during the chronic phase, along with a significant up-regulation in various inflammatory pathway-related genes (Weerasinghe-Mudiyanselage et al., 2022b). Previous research has documented the effects of inflammation on neuronal architecture of the striatum in EAE (Centonze et al., 2009; Rossi et al., 2009). However, comprehensive evidence-based reports on the structural plasticity of the hippocampus in EAE remain scarce. Furthermore, despite several studies on hippocampal neuroinflammation and synaptic plasticity in EAE, a detailed exploration of hippocampal structural plasticity in this animal model, crucial for understanding associated pathology and functional abnormalities, has not yet been conducted. To the best of our knowledge, the present study is the first to elucidate both neuronal structural plasticity and related molecular mechanisms in the EAE animal model, encompassing both acute and chronic stages.

Hippocampal neuroplasticity has been studied to assess its relationship with learning/memory-related and emotion-related behaviors across different animal models for various neurological disorders, including Alzheimer's disease (AD), Parkinson's disease (PD), and MS (Ang et al., 2021; Jiang et al., 2015; Kim et al., 2023; Stefanova et al., 2015; Weerasinghe-Mudiyanselage et al., 2021a, 2023). Many studies have shown a strong link between the neuronal structure and synaptic properties of the hippocampus and alterations in behavioral patterns and synaptic plasticity (Ma et al., 2019; McEwen, 2004). However, there is a gap in our understanding of certain changes in the structural plasticity of the hippocampus in experimental animal models of MS (Weerasinghe-Mudiyanselage et al., 2022a). Furthermore, the molecular mechanisms underlying hippocampal dysfunction in EAE remain largely unknown. Therefore, in the current study, we examined possible changes in structural plasticity of the hippocampus during autoimmune CNS inflammation induced by EAE, and further determined the potential involvement of major proinflammatory cytokines in these neuronal structural changes in the hippocampus.

MATERIALS AND METHODS

Animals and EAE induction

Adult male C57BL/6 mice (*n*=48) were obtained from Daihan Biolink Co. (Chungbuk, South Korea) at 9 weeks of age and allowed to acclimate for 1 week. All experimental and animal handling procedures were performed in accordance with the guidelines of the Institutional Care and Use Committee of Chonnam National University (CNU IACUC-YB-2022-102) and in line with the National Institute of Health's (NIH) Guide for the Care and Use of Laboratory Animals. Every effort was made to minimize the number of animals used and the suffering they experienced.

The induction of EAE in mice was performed as described previously (Weerasinghe-Mudiyanselage et al., 2022b). Briefly, mice in the EAE group were subcutaneously injected in the hind flank with 1 mg/mL of myelin oligodendrocyte glycoprotein (MOG_{35-55}) peptide (purity>96.44%; #051716, GL Biochem, China) emulsified in complete Freund's adjuvant (#F5881, Sigma-Aldrich, USA) and supplemented with 5 mg/mL *Mycobacterium tuberculosis* H37Ra (#BD231141, Difco Laboratories, USA). On day 0 and at 2 DPI, the mice were injected intraperitoneally with 500 ng of pertussis toxin (#181, List Biological Laboratories, USA). Mice in the control group were only injected with complete Freund's adjuvant without the MOG peptide. Following immunization, the experimental animals underwent daily weight checks and clinical scoring as follows: grade 0 (G.0), no signs; G.1, floppy tail; G.2, mild paraparesis; G.3, severe paraparesis; G.4, tetraparesis; G.5, moribund condition or death.

Open field test (OFT)

The OFT was performed as described previously (Wada et al., 2021; Yang et al., 2010) during the early and chronic phases of EAE. In each test, a mouse was first placed in the center of a brightly-lit arena (26 cm×26 cm, 250 lux) and allowed to explore for 30 min. Mouse activity was tracked using the TruScan Photo Beam Activity System (Coulbourn Instruments,

USA).

Golgi staining

The complexity of the hippocampal neuronal arbor and the quantity of dendritic spines were visualized using a Golgi staining technique, as previously outlined (Kim et al., 2022; Weerasinghe-Mudiyanselage et al., 2021a). Brain hemispheres (*n*=9/group) were washed in 0.1 mol/L phosphate buffer, submerged in Golgi-Cox solution for 14 days, then moved to a sucrose-containing solution at room temperature (RT; 22±2°C) for 3–7 days. The brains were sectioned (200 μm thickness) using a sliding microtome (SM2010R; Leica Microsystems, Germany) and mounted onto gelatin-coated slides. The slides were stored in the dark to air dry at RT for 3 days and processed for Golgi impregnation using a FD Rapid Golgistain™ Kit (#PK401, FD Neurotechnologies, USA) as instructed by the manufacturer.

Hippocampal neuronal tracing and Sholl analysis

Dendritic complexity, dendritic length, and number of branch points were quantified as described previously (Kim et al., 2022; Weerasinghe-Mudiyanselage et al., 2021a). Neuronal tracings were visualized at 200× using a Leica DM750 optical microscope (Leica Microsystems, Germany) and traced using the Leica Application Suite (v.4.12, Leica Microsystems, Germany) and Adobe Photoshop CS6 (Adobe Systems, USA). Sholl's concentric method (Sholl, 1953) and ImageJ (v.1.53f51, National Institutes of Health, USA) were used to analyze neuronal tracings. Ten neurons per hippocampal subregion were selected from each animal (*n*=9/group) using the criteria described by Morley & Mervis (2013): (1) Cell body was located in the subregion of interest, (2) branch staining was efficient and complete throughout the length, and (3) branches were isolated from their neighbors. Concentric circles were laid over the neuron starting from the cell body until the end of the longest dendrite at 10 μm intervals, and the number of dendrites intersecting at each circle was analyzed to determine complexity, length, and branch points. Ten neurons from each subregion were analyzed and averaged per mouse, with the mean number of each subregion of each mouse taken as *n*=1. The number per group was averaged and expressed as mean±standard error (SE). Sample size is indicated in the legends of the corresponding figures.

Analysis of dendritic spine density

Dendritic spine density was evaluated in the cornu ammonis 1 (CA1), CA3, and dentate gyrus (DG) subregions of the mouse hippocampus using an Olympus BX40 microscope (Tokyo, Japan) fitted with an eXcope X3 camera using the DIXI X3 v.5.0.1 program (DIXI Optics, South Korea). Constantly stained, unbranched, contiguous dendritic segments were selected for dendritic spine analysis. Dendritic spines were counted over 30 μm dendritic segments at a magnification of 1 500×. Five neurons from each hippocampal region were selected randomly from three consecutive brain sections from each animal, and two dendritic segments from each neuron were selected at the secondary and tertiary branch levels. Thus, for each animal, 10 segments were counted in total, and spine density was derived as the number of spines per 10 μm of dendritic length (Kang et al., 2018). The number of spines was averaged per mouse, with mean number of spines from each mouse taken as *n*=1. The number per group was averaged and expressed as mean±SE. Sample size is indicated in the legends of corresponding figures.

RNA extraction, cDNA synthesis, and reverse transcription quantitative real-time polymerase chain reaction (RT-qPCR)

RNA extraction, cDNA synthesis, and RT-qPCR were performed as described previously (Weerasinghe-Mudiyanselage et al., 2022b). RNA extraction from hippocampal tissue (*n*=5/group) was conducted using TRIzol reagent according to the manufacturer's instructions (#74106, Qiagen, Germany). Reverse transcription was performed using a Superscript™ III cDNA Synthesis Kit (#EZ405S, Enzynomics, South Korea). The resulting cDNA was diluted with RNase-free water to achieve a final concentration of 8 ng/μL, with the samples then stored at −70°C. RT-qPCR was performed using TOPreal™ SYBR Green qPCR PreMix (#RT500M, Enzynomics, South Korea) and the LineGene 9600 Plus system (BIOER, China) following the manufacturer's instructions. All RT-qPCR primers are listed in Table 1. The annealing temperature for the reaction was 58°C, and the built-in software generated the amplification curves and threshold cycle values. Glyceraldehyde-3-phosphate dehydrogenase (*Gapdh*) was used as the reference gene to normalize all readings. Data were expressed as mean relative values compared to the values of the control group via the $2^{-\Delta\Delta CT}$ method (Livak & Schmittgen, 2001).

Western blotting

Western blotting was performed as described previously (Wada et al., 2021; Weerasinghe-Mudiyanselage et al., 2021b). Each sample was sonicated for 10 s in buffer H (50 mmol/L β-glycerophosphate, 1.5 mmol/L ethylene glycol tetraacetic acid, 1 mmol/L dithiothreitol, 10 μg/mL aprotinin, 1 mmol/L phenylmethanesulfonyl fluoride, 0.1 mmol/L Na_3VO_4,

Table 1 Primer sequences used for RT-qPCR

Gene symbol	NCBI sequence	Primer pair (5'-3')	Length (bp)
Cd68	NM_009853	Forward- GGCGGTGGAATACAATGTGTCC Reverse- AGCAGGTCAAGGTGAACAGCTG	160
Gfap	NM_010277.1	Forward-CACCTACAGGAAATTGCTGGAGG Reverse-CCACGATGTTCCTCTTGAGGTG	136
Ifnγ	NM_008337.4	Forward-CAATCTTGCAGTCGTGTTTGTC Reverse- AGGGGATTACTGAGTGGCATC	312
Il1β	NM_008361.4	Forward-TGCCACCTTTTGACAGTGATG Reverse-ATGTGCTGCTGCGAGATTTG	136
Tnfα	NM_013693.3	Forward-CCCAAAGGGATGAGAAGTTCC Reverse-TGGGCTACAGGCTTGTCACTC	109
Gapdh	NM_008084	Forward-CATCACTGCCACCCAGAAGACTG Reverse-ATGCCAGTGAGCTTCCCGTTCAG	153

Cd68, cluster of differentiation 68; *Gfap*, glial fibrillary acidic protein; *Gapdh*, glyceraldehyde-3-phosphate dehydrogenase; *Ifnγ*, interferon gamma; *Il1β*, interleukin 1 beta; *Tnfα*, tumor necrosis factor alpha.

10 μg/mL leupeptin, and 2 μg/mL pepstatin; pH 7.4) before adding sodium dodecyl sulfate (SDS) sample buffer (6×) and heating at 100°C for 10 min. Proteins were separated by 10% SDS polyacrylamide gel electrophoresis (SDS-PAGE) (Bio-Rad, USA) and blotted onto polyvinylidene difluoride membranes (Amersham Hybond; GE Healthcare Life Sciences, USA). The membranes were blocked with 1% (v/v) normal goat serum (NGS; #S-1000, Vector Laboratories, USA) and 0.5% (v/v) bovine serum albumin (BSA; #A9647, Sigma-Aldrich, USA) in phosphate-buffered saline (PBS) containing 0.1% (v/v) Tween 20 (PBS-T; pH 7.4) for 1 h at RT. The membranes were then incubated with primary antibodies diluted in blocking serum: rabbit anti-phosphorylated-ERK (p-ERK) (1:2 000; #4376S, Cell Signaling, USA), rabbit anti-ERK (1:1 000; #4695S, Cell signaling, USA), or rabbit anti-ARC protein (1:1 000; #ab183183, Abcam, USA). After thorough washing, the membranes were incubated with horseradish peroxidase-conjugated anti-rabbit secondary antibody (1:5 000; #31460, Invitrogen, USA) for 1 h, before the signals were detected using the iBright^{TM} CL750 Imaging System (Thermo Fisher Scientific, USA) with a chemiluminescence kit (SuperSignal West Pico or Femto; Thermo Fisher Scientific, USA). The signals were normalized with β-actin detected with a mouse anti-β-actin primary antibody (1:5 000; Sigma-Aldrich, USA). Optical density (OD) per mm^2 and relative OD were calculated with respect to the corresponding β-actin intensity using ImageJ (NIH, USA). The mean intensity of the CON group was set to "1" in the respective immunoblots, and the proportional changes in intensity levels of each brain region were represented as relative OD fold changes. Relative OD was averaged group wise and represented as mean±SE.

Immunohistochemistry

All immunohistochemical procedures were carried out as reported previously (Ang et al., 2020; Kang et al., 2018). Fixed brain hemispheres were sectioned (thickness of 30 μm) in the coronal plane. Free-floating sections were incubated in 0.3% (v/v) hydrogen peroxide for 20 min prior to being blocked with 5% (v/v) NGS (Vector ABC Elite Kit; Vector Laboratories, USA) in 0.3% (v/v) Triton X-100 for 1 h at RT. The sections were incubated overnight at 4°C with rabbit anti-ARC antibody (1:1 000; #ab183183, Abcam, USA), then treated with biotinylated goat anti-rabbit IgG (Vector ABC Elite Kit, Vector Laboratories, USA) for 1 h at RT, followed by an avidin-biotin-peroxidase complex (Vector ABC Elite Kit; Vector Laboratories, USA) for 1 h at RT. Diaminobenzidine substrate (DAB kit; Vector Laboratories, USA) was added. For the negative control segments of each experiment, the primary antibody was not included.

The immunostained tissue sections were imaged using a Motic Easyscan Digital Slide Scanner (Motic, China). To qualify the intensity of ARC expression, three hippocampal hemisections (approximately 2.18 mm caudally from bregma) were chosen from each mouse. The quantification process was conducted in accordance with our established methodology, consistent with the approach employed in previous studies (Lee et al., 2016; Son et al., 2016). The following steps were implemented to ensure the precision and reliability of the intensity measurements: Images were first converted to 8-bit grayscale, and the threshold for each section was adjusted proportionally by subtracting the background to determine the immunoreactivity. The negative control sections (without primary antibodies) were used to set a single threshold for all sections for further correction. ImageJ (NIH, USA) was used to determine the mean gray value (across 256 gray levels) for each selected region. All measurements were consistently performed by the same individual blind to experimental conditions, ensuring enhanced consistency and minimizing potential observer bias. The mean intensity of immunoreactivity in the three sections of each mouse was set to n=1. After adjusting the mean intensity of the control to 1, the relative changes in intensity levels were represented as relative ARC ODs. Average intensity of the immunoreactivities per group was given as mean±SE (n=3 mice/group).

Cell culture and treatment

Primary hippocampal neurons were cultured as described previously (Ang et al., 2020). Hippocampi from C57BL/6J mouse pups at embryonic day 18 were used for culturing. Tissues were digested for 30 min at 37°C in dissociation buffer containing 10 units/mL papain (#LS003124, Worthington Biochemical, USA) and 100 units/mL DNase I (#04536282001, Roche Diagnostics GmbH, Germany). The solution was then triturated with Neurobasal A medium (#10888-022, Life Technologies, USA) into a single-cell suspension. The cells were then seeded at a density of 0.4×10^6 cells/well for western blotting and a density of 0.2×10^6 cells/well for immunofluorescence staining on poly-d-lysine hydrobromide (150 μg/mL; #P1024, Sigma-Aldrich, USA)-coated 24-well plates (Costar, China) with or without coverslips (12 mm; Marienfeld, Germany). Neurobasal A was replaced by Neurobasal A growth medium containing B27 supplement (#17504-044, Life Technologies, USA), 100 units/mL penicillin, 0.1 mg/mL streptomycin, and 0.5 mmmol/L glutamine (#10378-016, Life Technologies, USA) 1 h after plating. The cultures were incubated at 37°C and 5% CO_2. At 9 days *in vitro* (DIV), the cells were treated with Neurobasal A containing 10 ng/mL, 25 ng/mL, and 5 ng/mL of three proinflammatory cytokines (interleukin 1 beta (Il1β; #401-ML-005, R&D Systems, USA), tumor necrosis factor alpha (TNFα; #315-01A, PeproTech, USA), and interferon gamma (IFNγ; #50709-MNAH, Sino Biological, China)), respectively. The cytokine treatment protocol followed previous studies (Kim et al., 2002; Neumann et al., 2002; Rossi et al., 2014) and aimed to replicate the elevated levels of these three key proinflammatory cytokines observed *in vivo*. The control cells were only treated with Neurobasal A. After 24 h, the cells were analyzed biochemically or fixed for immunofluorescence staining.

Immunofluorescence

Primary neurons plated on coverslips were fixed with 4% paraformaldehyde solution for 20 min at RT. After washing with PBS, the cells were permeabilized with 0.2% Triton X-100 for 15 min. After blocking with 1% (v/v) NGS (Vector Laboratories, USA) and 0.5% (v/v) BSA (Sigma-Aldrich, USA) in PBS, mouse monoclonal anti-microtubule-associated protein 2 (MAP2; #M9942, Sigma, 1:200, USA) was added in antibody diluent to the cells for overnight incubation at 4°C. After three washes in PBS, the cells were incubated in anti-mouse Alexa Fluor-488 secondary antibody (#A10680, Life Technologies, 1:500, USA) in blocking solution for 1 h at RT. The nuclei on the immunofluorescence slides were counterstained with 4',6-diamidino-2-phenylindole (DAPI, #D1306, Thermo Fisher Scientific, 1:200, RRID:AB_2629482, USA). After three washes in PBS, coverslips were mounted

onto the glass slides using VECTORSHIELD Antifade Mounting Medium (#H-1400, Vector Laboratories, USA). The cells were visualized 72 h after initial staining. All images were taken within 7–10 days of coverslipping to minimize fading. Images were captured with a 200× immersion lens using an LSM 900 confocal laser-scanning microscope (Zeiss, Germany). MAP2-immunoreactive dendritic arbors were traced using Adobe Photoshop CS6 (Adobe Systems, USA) and analyzed using the Sholl concentric circle method, as described above.

Cytotoxicity assessment

Cytotoxicity in the hippocampal-cultured neurons was assessed using a lactate dehydrogenase (LDH) release assay (#K313-500, LDH Cytotoxicity Assay Kit, Biovision, USA; n=4 cultures for four separate conditions). The assay was performed following the manufacturer's recommendations, and OD at 450 nm was determined using a microplate reader (BioTek Epoch-SN; Agilent, USA) and GEN5 (v.3.12.08).

Statistical analysis

All statistical analyses were performed using GraphPad (v.9.3.1, GraphPad Software, USA). Two-way analysis of variance (ANOVA) followed by Sidak's multiple comparisons test was performed to analyze dendritic complexity and spine density between control (CON) and EAE-affected/cytokine-treated groups. Unpaired Student's t-test was applied to compare all other experimental results between the CON and EAE-affected/cytokine-treated groups. For all statistical tests, P<0.05 was considered significant. All data are represented as mean±SE. The number of samples used for each experiment are mentioned in the respective results sections and figure legends.

RESULTS

Clinical score following immunization

After EAE induction with the MOG_{35-55} peptide, the mice were monitored daily for clinical score and body weight until 28 DPI. Flaccid tails were observed at 12 DPI and hind limb paralysis was observed at approximately 15–24 DPI (Figure 1A). By 28 DPI, the EAE-affected mice had recovered from hind limb paralysis and showed chronic tail atony ($F_{interaction}$ (28, 638)=35.98, P<0.001; Figure 1A). Following behavioral tests at 11 and 28 DPI, samples were collected for Golgi staining and biochemical analyses.

Hypolocomotion and anxiety-like behavior in EAE mice

EAE animal models have previously been used to evaluate non-motor symptoms during the early and chronic phases (Acharjee et al., 2013; Dutra et al., 2013; Kim et al., 2012). However, the presence of motor symptoms can hinder the interpretation of non-motor behavioral changes (Seibenhener & Wooten, 2015). Hence, to confirm the existence of motor symptoms before the development of clinical disease, as well as after the resolution of major clinical symptoms in the chronic EAE model, the mice were subjected to OFT during the early (11 DPI) and chronic (28 DPI) phases (n=12 mice/group; Figure 1B, C). In agreement with our hypothesis, total distance traveled in the open field was lower in the EAE-affected group during both the early (CON: 6 224±286, EAE: 1 600±172; t(22)=13.860, P<0.001; Figure 1B) and chronic (CON: 4 544±332, EAE: 1 807±142; t(22)=7.593, P<0.001; Figure 1C) phases of EAE. Moreover, while the percentage of distance traveled in the central area was significantly reduced in the early phase of EAE (CON: 41.84±2.31, EAE: 25.16±2.18; t(22)=5.251, P<0.001), time spent in the central area did not differ significantly between the CON and EAE mice in the early phase (Figure 1B). During the chronic phase of EAE, both the percentage of time spent in the central area (CON: 46.61±1.27, EAE: 18.42±4.98; t(22)=5.481, P<0.001) and distance traveled (CON: 49.99±1.52, EAE: 26.21±5.76; t(22)=3.993, P<0.001) were significantly lower in the EAE group compared to the CON group (Figure 1C).

Changes in dendritic complexity in EAE-affected hippocampi

Hippocampal dendritic complexity changes and hippocampus-related behavioral disturbances are known to coexist in neurodegenerative and neuroinflammatory conditions (Liu et al., 2020; Planche et al., 2017; Weerasinghe-Mudiyanselage et al., 2022a). However, such evidence from EAE-affected brains remains limited. Therefore, to determine whether hippocampal structural plasticity underpins the behavioral changes observed in EAE-affected mice, we analyzed the dendritic complexity of neurons in the hippocampal CA1, CA3, and DG subregions based on number of crossing dendrites, total dendritic length, and number of branch points per neuron. During the early phase after EAE induction in the hippocampal CA1, CA3, and DG subregions, the dendritic intersections at different radial distances from the neuronal soma were counted using Sholl analysis (n=9 mice/group; Figure 2). In the CA1 apical subregion, significantly fewer dendritic intersections were observed in the EAE-affected group than in the CON group at Sholl radii of 240–330 μm from the soma ($F_{interaction}$ (41,672)=2.883, P<0.001; Figure 2B, line graphs). Total dendritic length was also shorter in the EAE-affected group (CON: 3 144±78, EAE: 2 736±99; t(16)=3.235, P=0.0052; Figure 2B, left bar graphs). In the CA1 basal (Figure 2C) and CA3 subregions (Figure 2E, F), no significant differences in dendritic complexity were found between the CON and EAE-affected groups. In the DG subregion, there were fewer branch points/neurons in the EAE-affected group (CON: 7.644±0.238, EAE: 6.844±0.234; t(16)=2.396, P=0.0291; Figure 2H, right bar graphs), without any significant change in the number of dendritic crossings and total dendritic length (Figure 2H, left bar graphs).

In the chronic phase of EAE, hippocampal dendritic complexity was extensively affected in the CA1, CA3, and DG subregions (n=9 mice/group; Figure 3). In the CA1 apical region, significantly fewer dendrite intersections were observed in the EAE-affected mice than in the CON group at Sholl radii of 220–340 μm from the soma ($F_{interaction}$ (39,640)=3.295, P<0.001; Figure 3B). Furthermore, there were fewer dendritic intersections in the CA1 basal subregion in the EAE group compared to the CON group at Sholl radii of 100–140 μm from the soma ($F_{interaction}$ (17,288)=2.767, P=0.003; Figure 3C). In the CA3 apical region, significantly fewer dendrite intersections were found in the EAE-affected mice than in the CON group at Sholl radii of 90–190 μm from the soma ($F_{interaction}$ (40,656)=4.605, P<0.001; Figure 3E). There were also fewer dendritic intersections in the CA3 basal subregion of the EAE group than of the CON group at Sholl radii of 70–180 μm from the soma ($F_{interaction}$ (40,656)=8.983, P<0.001; Figure 3F). Similarly, in the DG subregion, the number of dendritic intersections was significantly reduced in the EAE group compared to the CON group at Sholl radii of 150–180 μm from the soma ($F_{interaction}$ (24,400)=2.083,

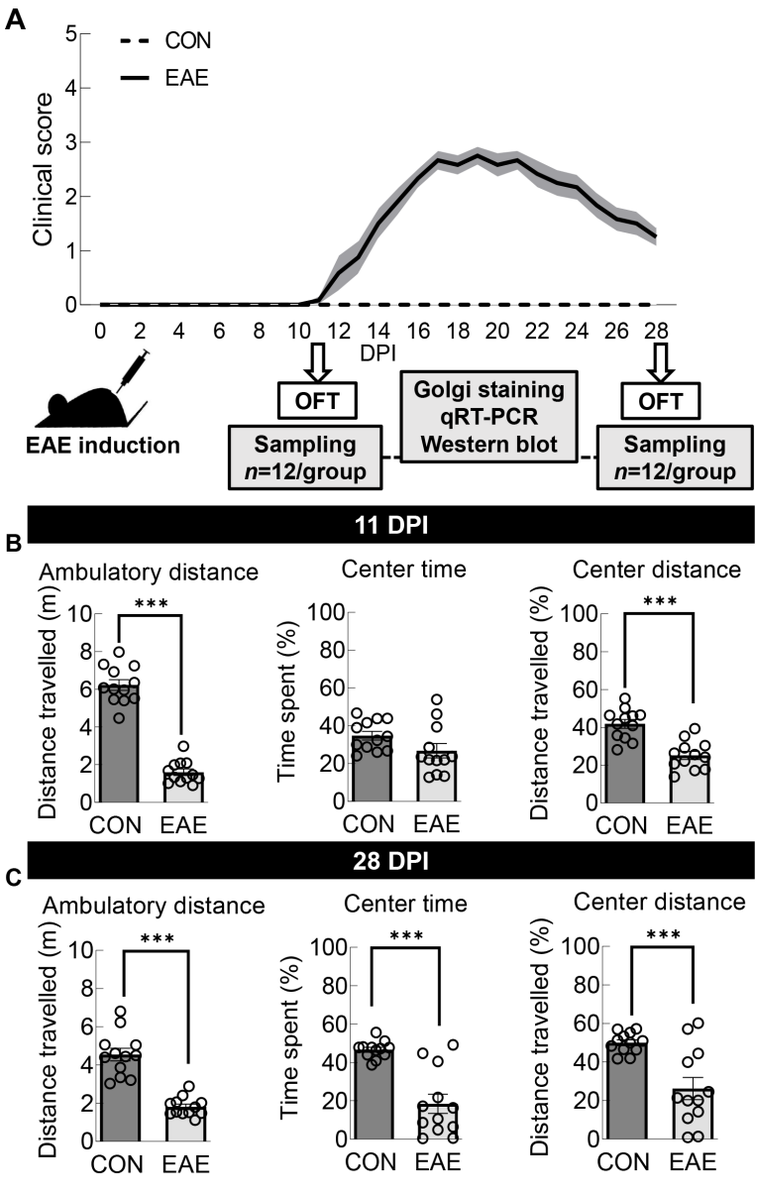

Figure 1 Schematic of experimental design and behavioral changes during early and chronic phases of EAE

A: After induction of EAE, clinical score was recorded daily, open field test (OFT) was performed at 11 and 28 days post-immunization (DPI), and animals were sacrificed to obtain samples for Golgi staining, RT-qPCR, western blotting, and immunohistochemistry. B, C: Bar graphs show ambulatory distance, percentage of time spent in central area, and percentage of distance traveled in central area of the open field during early (B) and chronic phases (C) of EAE. Data are combined mean±SE of two separate experiments (*n*=12/group). Gray zone in the line graph signifies standard error of the mean. **: *P*<0.01, ***: *P*<0.001 vs. CON group.

P=0.0023; Figure 3H).

During the chronic phase of EAE, total dendritic length was significantly reduced in the CA1 apical (CON: 1 701±84, EAE: 1 340±58; *t*(16)=3.544, *P*=0.0027; Figure 3B, left bar graphs) and basal (CON: 921±20, EAE: 777±31; *t*(16)=3.883, *P*=0.0013; Figure 3C, left bar graphs), CA3 apical (CON: 1 163±67, EAE: 831±67; *t*(16)=3.500, *P*=0.003; Figure 3E, left bar graphs) and basal (CON: 932±66, EAE: 592±31; *t*(16)=4.648, *P*<0.001; Figure 3F, left bar graphs), and DG subregions (CON: 2 481±76, EAE: 2 192±46; *t*(16)=3.246, *P*=0.0051; Figure 3H, left bar graphs). In the CA3 region, the number of branching points per neuron was reduced in the apical (CON: 8.856±0.578, EAE: 6.689±0.436; *t*(16)=2.992, *P*=0.0086; Figure 3E, left bar graphs) and basal (CON: 7.133±0.493, EAE: 5.010±0.369; *t*(16)=3.446, *P*=0.0033; Figure 3F, left bar graphs) subregions of the EAE group. In the DG region, branch points per neuron were significantly reduced in the EAE group compared to the CON group (CON: 7.644±0.238, EAE: 6.844±0.234; *t*(16)=2.396, *P*=0.0291; Figure 3H, right bar graphs). However, the number of branching points per neuron was not significantly affected in the CA1 apical and basal subregions in the EAE group (Figure 3B, C, right bar graphs). Taken together, these findings indicate that dendritic complexity is primarily affected during the chronic phase of EAE, with minimal effects during the early phase.

Changes in dendritic spine density in EAE-affected hippocampi

Dendritic spines constitute the major components of synapses between hippocampal neurons, with rapid modifications in these structures observed in many neurodegenerative disorders (Bellot et al., 2014; Moolman et al., 2004; Tsai et al., 2020; Weerasinghe-Mudiyanselage et al., 2021a). Therefore,

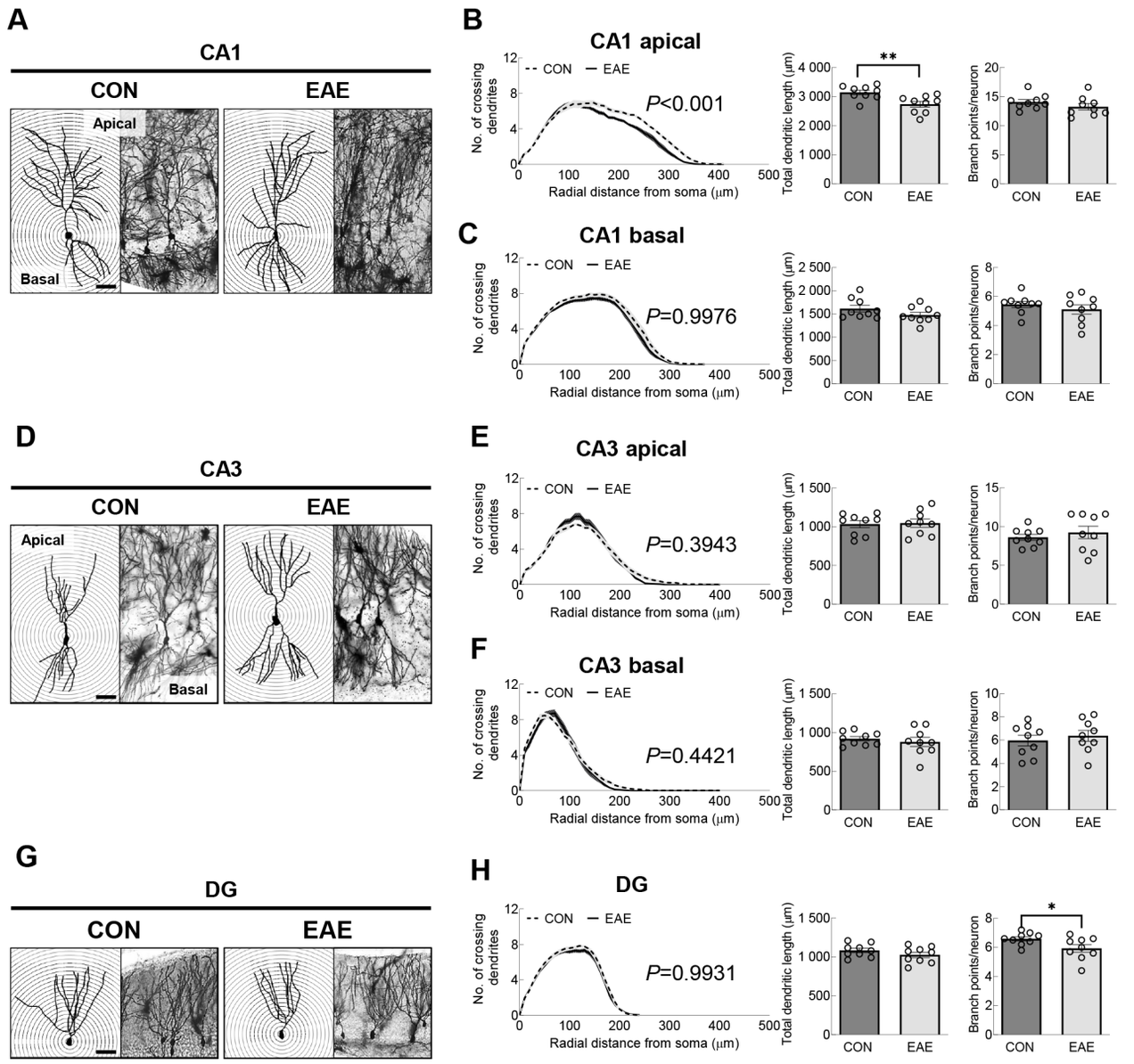

Figure 2 Dendritic complexity of hippocampal neurons in each subregion during early phase of EAE

A–H: Photographs show CA1 (A), CA3 (D), and DG (G) neurons with overlaid concentric circles used for Sholl analysis. Line graphs show mean number of intersections per 10 μm radial unit distance from the soma (0) for dendrites in the CA1 apical (B) and basal (C), CA3 apical (E) and basal (F), and DG subregions (H). Bar graphs display total dendritic length (left panel) and dendritic branch points (right panel) per neuron in each subregion. Data are combined mean±SE of two separate experiments (10 neurons per mouse, n=9 mice/group). Gray zones in line graphs signify standard errors of the means. *: P<0.05, **: P<0.01 vs. CON group. Scale bars represent 50 μm.

we also explored possible changes in dendritic spine density in the hippocampal CA1, CA3, and DG subregions of EAE-affected mice (n=9 mice/group; Figure 4). Results showed that spine density in the EAE-affected group was significantly reduced during the early phase in the CA1 apical (CON: 17.99±0.79, EAE: 13.49±0.52; t(16)=4.766, P<0.001; Figure 4A), CA1 basal (CON: 16.89±1.32, EAE: 12.40±0.62; t(16)=3.073, P=0.0073; Figure 4B), CA3 apical (CON: 13.98±0.48, EAE: 12.36±0.58; t(16)=2.154, P=0.0047; Figure 4C), CA3 basal (CON: 15.44±0.24, EAE: 12.18±0.58; t(16)=5.189, P<0.001; Figure 4D), and DG subregions (CON: 21.11±1.1, EAE: 14.03±0.80; t(16)=5.237, P<0.001; Figure 4E). In the chronic phase of EAE, spine density was significantly reduced in the CA3 apical (CON: 15.09±0.44, EAE: 13.13±0.35; t(16)=3.505, P=0.0029; Figure 4H), basal (CON: 14.67±0.28, EAE: 12.04±0.53; t(16)=4.416, P<0.001; Figure 4I) and DG region (CON: 20.46±1.76, EAE: 15.95±0.69; t(16)=2.385, P=0.0298; Figure 4I), but not in the CA1 apical and basal subregions (Figure 4F, G). Collectively, these results imply that changes in spine density in the hippocampus are more likely to occur in the early phase of EAE, rather than in the chronic phase.

Changes in mRNA levels of proinflammatory cytokines and markers in EAE-affected hippocampi

EAE induces inflammation within the CNS (Kim et al., 2019; Pierson et al., 2012; Zorzella-Pezavento et al., 2013). We

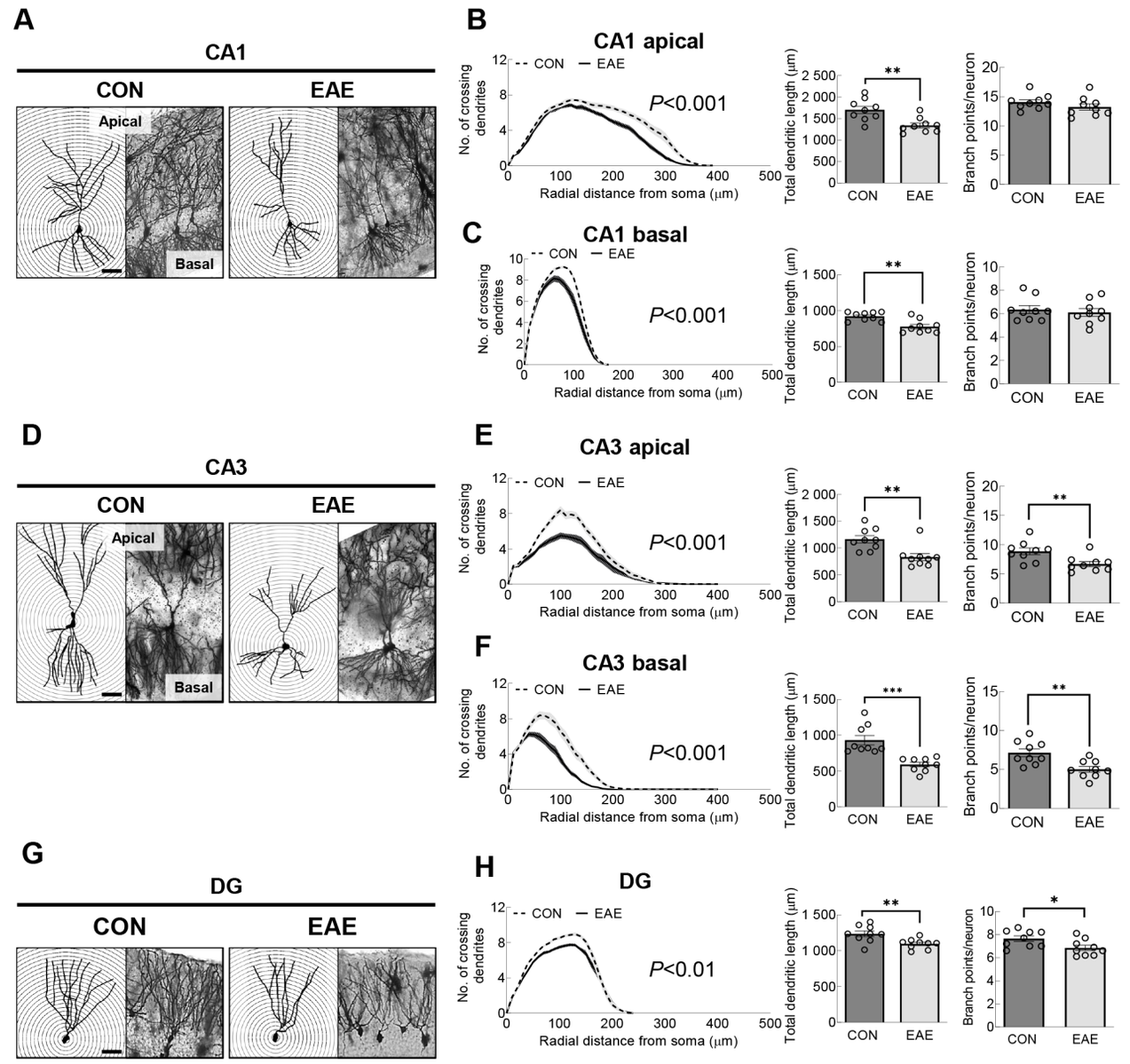

Figure 3 Dendritic complexity of hippocampal neurons in each subregion during the chronic phase of EAE

A–H: Photographs show CA1 (A), CA3 (D), and DG (G) neurons with overlaid concentric circles used for Sholl analysis. Line graphs show mean number of intersections per 10 μm radial unit distance from the soma (0) for dendrites in the CA1 apical (B) and basal (C), CA3 apical (E) and basal (F), and DG subregions (H). Bar graphs display total dendritic length (left panel) and dendritic branch points (right panel) per neuron in each subregion. Data are combined mean±SE of two separate experiments (10 neurons per mouse, n=9 mice/group). Gray zones in line graphs signify standard errors of the means. *: P<0.05, **: P<0.01, ***: P<0.001 vs. CON group. Scale bars represent 50 μm.

previously documented inflammatory pathway activation in the hippocampus during the chronic phase of EAE (Weerasinghe-Mudiyanselage et al., 2022b). Furthermore, EAE animal models have shown that neuroinflammation can significantly impact hippocampal synaptic plasticity (Nisticò et al., 2013; Rizzo et al., 2018). Here, the mRNA levels of proinflammatory cytokines were investigated to determine the extent of neuroinflammation in the hippocampi during the early and chronic phases of EAE (n=5 mice/group; Figure 5). Results showed that the mRNA levels of proinflammatory cytokines, astrocyte markers, and activated microglial/macrophage markers in EAE-affected hippocampi were significantly elevated in the chronic phase (Figure 5B), but not in the early phase (Figure 5A): *Il1β* (CON: 1.000±0.074, EAE: 3.131±0.738; t(8)=2.874, P=0.0207), *Tnfα* (CON: 1.000±0.156, EAE: 24.210±3.246; t(8)=7.141, P<0.001), *Ifnγ* (CON: 1.000±0.233, EAE: 4.155±1.262; t(8)=2.459, P=0.0394), *Cd68* (CON: 1.000±0.092, EAE: 2.043±0.343; t(8)=2.935, P=0.0188), and *Gfap* (CON: 1.000±0.105, EAE: 1.987±0.271; t(8)=3.391, P=0.0095). Taken together, these observations indicate the presence of pronounced inflammation during the chronic phase of EAE, potentially driven by activated astrocytes and macrophage-lineage cells.

Decreased expression of ARC in hippocampi during the chronic phase of EAE

We next sought to unravel the molecular mechanism driving

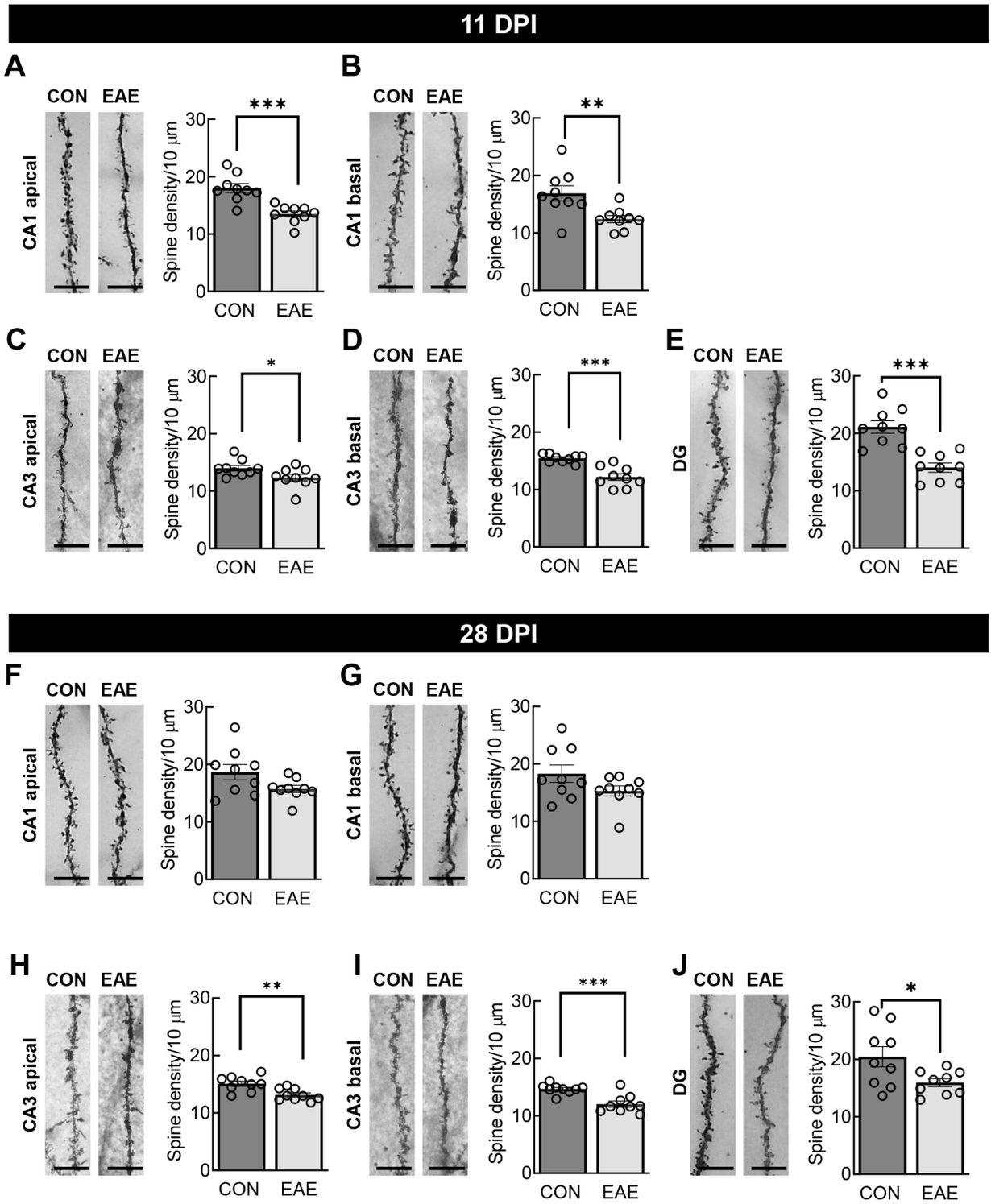

Figure 4 Dendritic spine density of hippocampal neurons in each subregion during early and chronic phases of EAE

A–J: Bar graphs (A–E) and (F–J) display spine density per 10 μm dendrite length during early and chronic phases of EAE, respectively. Data are combined mean±SE of two separate experiments (10 dendritic segments per mouse, n=9 mice/group). *: P<0.05, **: P<0.01, ***: P<0.001 vs. CON group. Scale bars represent 5 μm.

the observed structural changes in the EAE-affected mouse hippocampi. Previously, we reported a reduction in mRNA levels of immediate early genes (IEGs), including *Arc*, early growth response 1 (*Egr1)*, transcription factor Jun-B (*Junb*), and Fos proto-oncogene (*Fos*), in the hippocampi of EAE-affected mice during the chronic phase (Weerasinghe-Mudiyanselage et al., 2022b). ARC is colocalized with the actin cytoskeletal matrix, a major constituent of dendrites (Lyford et al., 1995). Thus, in the present study, we measured the protein levels of ARC in the hippocampi of EAE-affected mice during the chronic phase (n=4 mice/group; Figure 6A). Results demonstrated that the expression of ARC in the hippocampi of EAE-affected mice was significantly reduced compared to that in the CON group (CON: 1.000±0.107, EAE: 0.463±0.060; t(6)=4.384, P=0.0047). Immunostaining further characterized the reduced expression of ARC in hippocampal

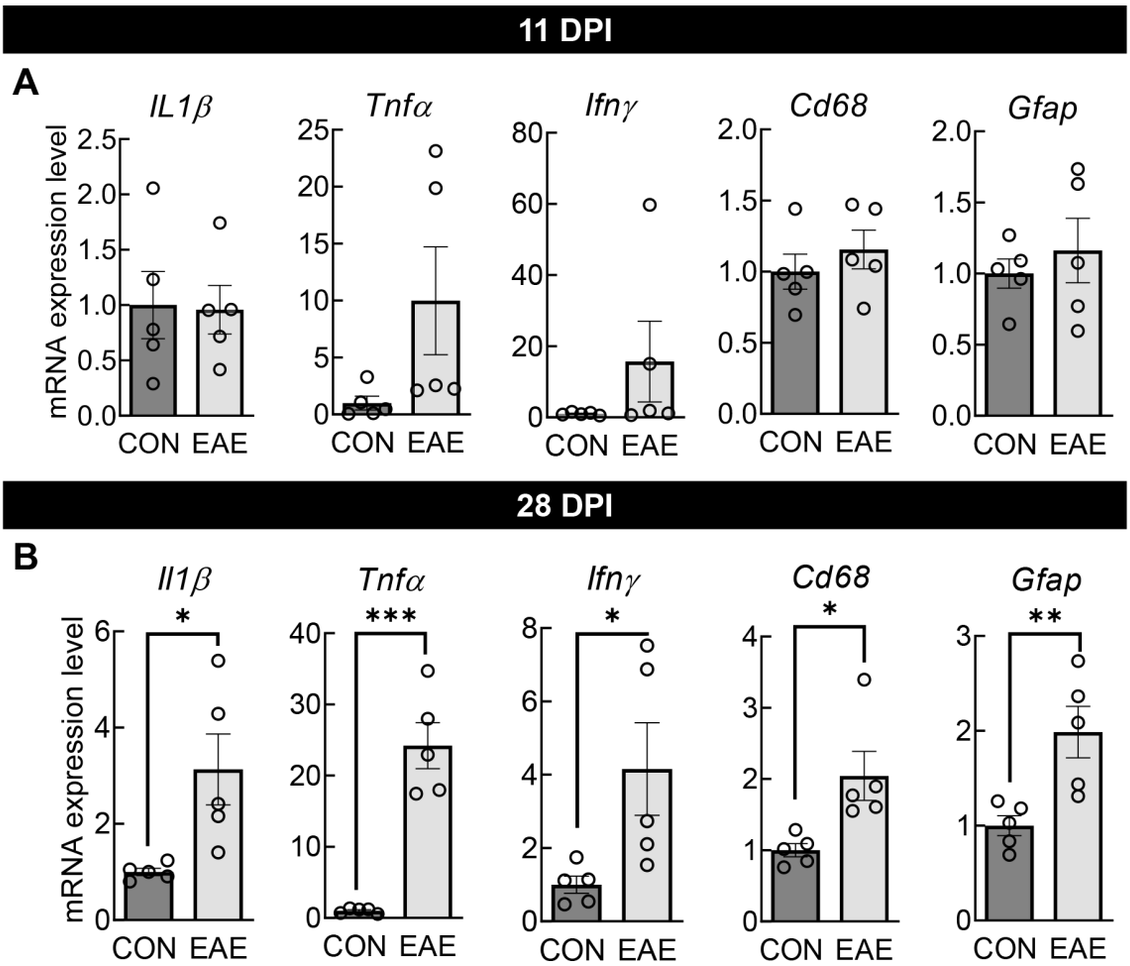

Figure 5 mRNA levels of proinflammatory markers in the hippocampus of EAE-affected mice

A, B: Bar graphs represent relative mRNA levels of *Il1β*, *Tnfα*, *Ifnγ*, *Cd68*, and *Gfap* at 11 DPI (early phase, panel A) and 28 DPI (chronic phase, panel B) based on RT-qPCR. Data are combined mean±SE of two separate experiments (n=5 mice/group). *: P<0.05, **: P<0.01, ***: P<0.001 vs. CON group. *Cd68,* cluster of differentiation 68; DPI, days post-immunization; EAE, experimental autoimmune encephalomyelitis; *Gfap,* glial fibrillary acidic protein; *Ifnγ,* interferon gamma; *Il1β,* interleukin 1 beta; *Tnfα,* tumor necrosis factor alpha.

subregions (n=3 mice/group; Figure 6B), with extensive localization of ARC expression across the hippocampus. Specifically, the expression levels of ARC in the CA1 (CON: 1.000±0.036, EAE: 0.709±0.079; t(4)=3.355, P=0.0284), CA3 (CON: 1.000±0.051, EAE: 0.790±0.047; t(4)=3.006, P=0.0397), and DG subregions (CON: 1.000±0.015, EAE: 0.857±0.047; t(4)=2.893, P=0.044) were lower in the EAE group that in the CON group. Collectively, the expression patterns of ARC in the hippocampi of EAE-affected mice are consistent with the neuronal structural changes in this brain region and higher levels of proinflammatory markers during the chronic phase. These results suggest that the profound neuroinflammation observed during the chronic phase of EAE may affect hippocampal neuronal structural plasticity through ARC expression.

Treatment with proinflammatory cytokines significantly decreased dendritic complexity in primary cultures of hippocampal neurons

Next, we further explored the detrimental effects of proinflammatory cytokines on the dendritic arborization of hippocampal neurons. According to previous studies, proinflammatory cytokines can induce changes in the structural plasticity of CNS neurons *in vitro* (Gilmore et al., 2004; Kim et al., 2002). Therefore, we carried out *in vitro* experiments to exogenously treat cells with three cytokines (Il1β, Tnfα, and Ifnγ) highly expressed in the hippocampus during the chronic phase of EAE. Results showed that treatment with proinflammatory cytokines significantly reduced dendritic complexity in the primary hippocampal neuronal cultures (n=9/group; Figure 7A–E). There was a significant reduction in the number of dendritic intersections in the cytokine-treated group (Cytokine) at Sholl radii of 80–260 per 10 μm from the soma ($F_{\text{interaction}}$ (39,640)=9.293, P<0.001; Figure 7C). Moreover, total dendritic length (CON: 1 431±37, Cytokine: 852±48; t(16)=9.520, P<0.001; Figure 7D) and branch points per neuron (CON: 7.611±0.454, Cytokine: 5.611±0.274; t(16)=3.772, P=0.0017; Figure 7E) were lower in the Cytokine group than in the CON group. However, proinflammatory cytokine treatment did not damage primary hippocampal neurons, as shown by the LDH assay (n=16/group; Figure 7F). Overall, these *in vitro* experiments confirmed the proinflammatory cytokine-induced reduction of dendritic complexity in hippocampal neurons.

Treatment with proinflammatory cytokines significantly decreased ERK phosphorylation and ARC expression in primary cultures of hippocampal neurons

We also sought to clarify how inflammation may induce changes in structural plasticity. Consistent with the reduction

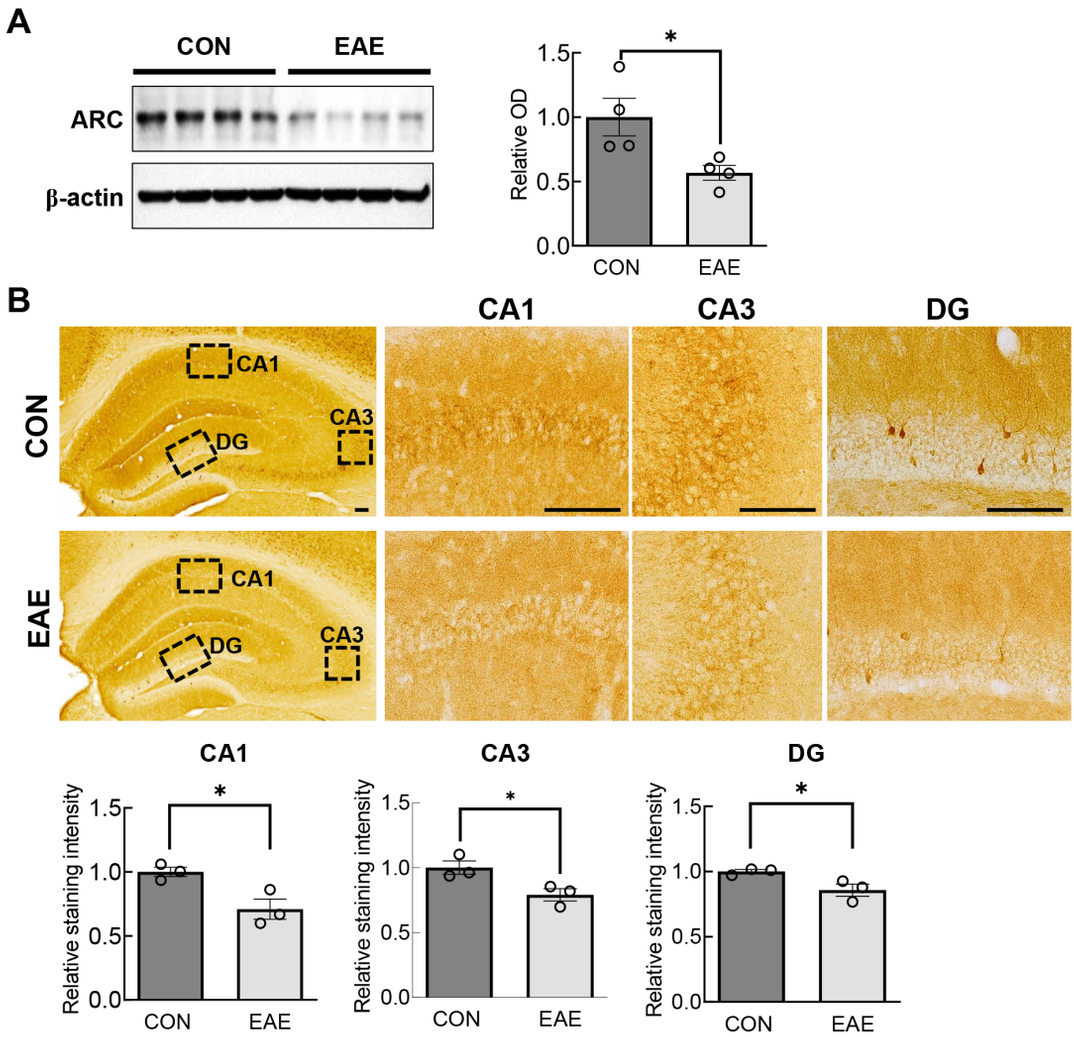

Figure 6 ARC expression in the hippocampus during chronic phase of EAE

A: Representative western blot image and bar graph representing relative levels of ARC in the hippocampus during chronic phase of EAE (*n*=4 mice/group). B: Representative immunohistochemical photographs and immunoreactivity of ARC in CA1, CA3, and DG subregions of the hippocampus during chronic phase of EAE. (*n*=3mice/group). Data are combined mean±SE of two separate experiments *: *P*<0.05 vs. CON group. Scale bars represent 200 μm and 100 μm in (B) left and right panels, respectively. ARC, activity-regulated cytoskeleton-associated protein; CA1, cornu ammonis 1; CA3, cornu ammonis 3; DG, dentate gyrus; DPI, days post-immunization; EAE, experimental autoimmune encephalomyelitis.

in ARC expression in the mouse hippocampi during the chronic phase of EAE, cytokine treatment also significantly reduced the expression levels of ARC in primary cultures of hippocampal neurons (*n*=4/group; Figure 7G) (CON: 1.000±0.019, Cytokine: 0.596±0.041; *t*(6)=8.843, *P*<0.001). Transcriptional activity of *Arc* is controlled by the ERK signaling pathway (Murphy et al., 2002), which is widely reported to play a key role in neuroinflammation (Lee et al., 2016). Therefore, changes in p-ERK/ERK activation levels were determined in cytokine-treated hippocampal neurons (*n*=4/group; Figure 7G). Results showed that cytokine treatment significantly reduced ERK phosphorylation levels in primary cultures of hippocampal neurons (p-ERK1; CON: 1.000±0.135, EAE: 0.254±0.046; *t*(6)=5.218, *P*=0.002 and p-ERK2; CON: 1.000±0.024, EAE: 0.427±0.043; *t*(6)=11.60, *P*<0.001, Figure 7G). Collectively, these findings suggest that the ERK-ARC pathway may mediate the observed cytokine-mediated structural changes in hippocampal neurons.

DISCUSSION

In this study, we examined alterations in neuronal architecture and explored potential mechanisms in the hippocampi of mice with EAE during the early and chronic phases, critical periods for neuroplasticity assessments and investigating non-motor behavioral changes. Results showed that the EAE-affected mice exhibited hypolocomotion and anxiety-like behavior, with marked effects on hippocampal structural plasticity, primarily during the chronic phase. This change in dendritic complexity was accompanied by a significant increase in proinflammatory mediators and a reduction in the expression of ARC during the chronic phase of EAE. Exogenous treatment of primary cultures of hippocampal neurons with proinflammatory cytokines suppressed dendritic arborization, possibly through the ERK-ARC pathway.

Cognitive impairment and emotional dysregulation associated with hippocampal dysfunction are frequently reported in MS patients (Ko et al., 2021; Rocca et al., 2018), and can be recapitulated to varying extents in experimental models of MS (Di Filippo et al., 2016; Haji et al., 2012). In this study, EAE-affected mice exhibited anxiety-like symptoms during both the early and chronic phases, as evidenced by reduced time spent and distance traveled in the central area of

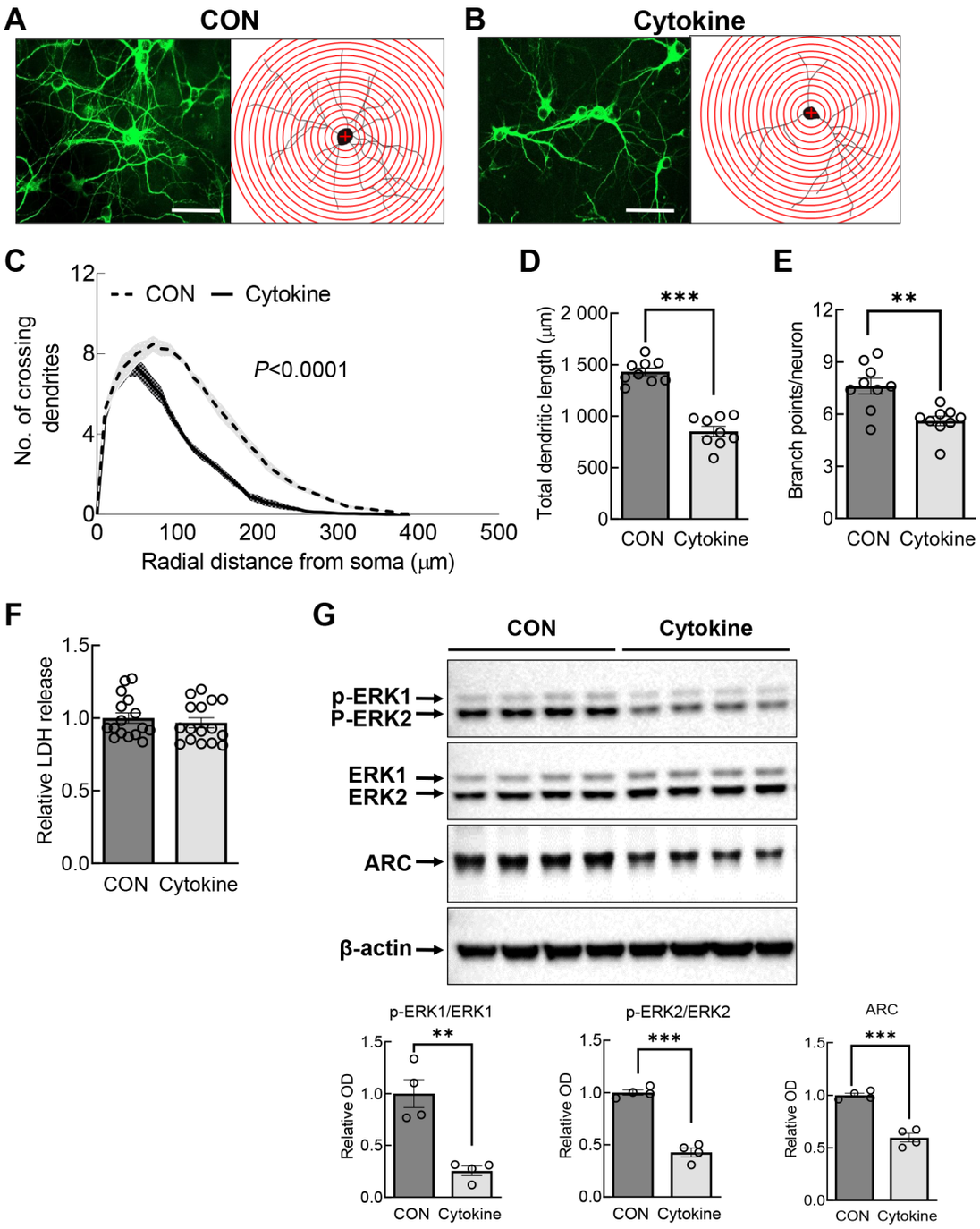

Figure 7 Dendritic complexity, ERK phosphorylation, and ARC expression in primary cultures of hippocampal neurons following treatment with proinflammatory cytokines

A, B: MAP2 staining of neurons from CON (A) and Cytokine (Il1β+Tnfα+Ifnγ-treated) (B) groups revealed significant reduction of dendritic complexity in cytokine-treated neurons. C: Line graphs show mean number of intersections per 10 μm radial unit distance from the soma (0) for dendrites in primary hippocampal neurons at 10 DIV. D, E: Bar graphs display (D) total dendritic length and (E) dendritic branch points per neuron (*n*=9/group). F: Bar graphs show relative LDH release from primary cultured hippocampal neurons following cytokine treatment (*n*=16/group). G: Bar graphs display relative expression level of p-ERK1, p-ERK2, and ARC after cytokine treatment in hippocampal neurons (*n*=4/group). Data are combined mean±SE of two separate experiments. **: *P*<0.01, ***: *P*<0.001 vs. CON group. Scale bars represent 50 μm. ARC, activity-regulated cytoskeleton-associated protein; DIV, days in vitro; ERK, extracellular signal-regulated kinases; Ifnγ, interferon gamma; Il1β, interleukin 1 beta; LDH, lactate dehydrogenase; Tnfα, tumor necrosis factor alpha.

the open field. However, it is crucial to note that these EAE mice exhibited persistent locomotor deficits, even in the absence of major clinical signs during the early phase and after resolution of prominent clinical symptoms in the chronic phase. Thus, to mitigate the potential confounding impact of motor dysfunction on the interpretation of anxiety-like behavior, we utilized the percentages of time and distance traveled in the central area of the open field as measures of anxiety-like symptoms. Given the presence of motor dysfunction in both phases, additional behavioral assessments using specific paradigms were not performed on the mice in order to prevent misinterpretation of results due to the

influence of motor impairments. By focusing on the percentages of time and distance in the central area, we aimed to provide a more accurate representation of anxiety-like symptoms while considering the inherent motor deficits associated with the EAE model.

Various brain regions, including but not limited to the hippocampus, prefrontal cortex, amygdala, thalamus, and hypothalamus, regulate neuropsychiatric and cognitive behaviors. Given the complexity of covering such a wide array of regions, our experiments focused primarily on the hippocampus, particularly given its reported involvement in the pathogenesis of MS (Rocca et al., 2018; Zheng et al., 2022). Although we did not assess cognitive function in this particular EAE animal model due to potential confounding motor dysfunction, patients with MS often exhibit cognitive dysfunction and depressive pathologies, which are closely associated with hippocampal lesions (Colasanti et al., 2016). In future studies, we will explore the roles of the amygdala and other relevant brain regions in the regulation of different functional aspects in this animal model.

As a major brain region that regulates cognitive and emotional behavior, the hippocampus has been studied for possible neuroarchitectural changes in terms of dendritic complexity and spine density (Kim et al., 2022; Weerasinghe-Mudiyanselage et al., 2021a). To the best of our knowledge, however, this study represents the first extensive analysis of structural changes in hippocampal neurons during the early and chronic phases of the disease. Notably, major changes in dendritic complexity were observed during the chronic phase, while significant changes were only observed in the CA1 apical subregion during the early phase. The data revealed a consistent pattern of reduction in dendritic complexity at various distances from the soma, as well as in decreases in dendritic length and branch points across all examined subregions. Although not all findings reached statistical significance, these trends suggest that alterations in neuronal structural plasticity in this animal model may begin as early as the acute phase and progressively intensify as the disease progresses toward the chronic phase. Previous research has reported the loss of synaptic connections in the CA3 and CA1 subregions in mice with EAE (Michailidou et al., 2015), as well as reduced volumes in the CA3 subregion of MS patients with depressive symptoms (Gold et al., 2010), supporting our findings of reduced neuronal activity in this subregion. Given that CA1 apical dendrites receive massive projections from the Schaffer collaterals of CA3 neurons (Ishizuka et al., 1990; Li et al., 1994), diminished neuronal activity in CA3 and its projections may result in reduced dendritic length in the CA1 subregion. The unique DG subregion of the hippocampus is known for its role in adult neurogenesis (Boldrini et al., 2018) and notable changes in plasticity under different pathological and physiological conditions (Weerasinghe-Mudiyanselage et al., 2022a). Selective disruption of DG subregion neuroplasticity during the early phase of EAE has been reported in animal models, together with memory impairment (Di Filippo et al., 2013; Planche et al., 2017). Patients with MS have also shown significant hippocampal volume reductions, initially in the CA1 during the early phase and later extending to the DG subregion during the chronic phase (Sicotte et al., 2008). Collectively, the observed changes in neuronal plasticity across the different hippocampal subregions appear to vary during the progression of EAE and MS. Furthermore, the diversity in EAE induction protocols, leading to varying degrees of disease severity, may also account for the contrasting observations in EAE animal models (Novkovic et al., 2015). Nevertheless, it is crucial to acknowledge that our analysis of inflammatory cytokines was conducted on a global level, without assessing localized expression in different subregions of the hippocampus during the early phase. The lack of significant findings for major proinflammatory cytokines does not exclude the possibility of changes in other inflammatory molecules within specific hippocampal subregions, which could potentially influence neuronal architecture. Additionally, our focus on mRNA expression levels to evaluate cytokine dynamics in the EAE model represents a limitation. Complementing these findings with protein-level analysis is necessary for a more comprehensive understanding. Consequently, while our study revealed substantial changes in mRNA expression, with more than a 2-fold increase for all proinflammatory cytokines, future investigations incorporating techniques such as enzyme-linked immunosorbent assay (ELISA) with mouse cerebrospinal fluid will be instrumental in providing valuable insights into the translational relevance of these observed mRNA changes.

Persistent neuroinflammation is described as a frontline cause for synaptic plasticity changes in MS and EAE (Weerasinghe-Mudiyanselage et al., 2022a). In the present study, the reduction in dendritic complexity during the chronic phase of EAE was also associated with increased proinflammatory cytokine levels, implying a direct impact of neuroinflammation degree on dendritic arborization. Furthermore, primary cultures of hippocampal neurons showed a significant reduction in dendritic complexity upon exogenous cytokine treatment. This is consistent with other reports demonstrating impaired hippocampal synaptic plasticity along with increased levels of inflammatory mediators and reactive gliosis in CNS with EAE (Centonze et al., 2010; Di Filippo et al., 2013; Nisticò et al., 2013). Moreover, a previous study on EAE-affected mice also revealed an association between dendritic abnormalities in spinal cord motor neurons and local infiltration of inflammatory cells (Bannerman et al., 2005). Chronic neuroinflammation alters dendritic arborization, even in neuroinflammatory conditions other than MS/EAE. For example, neuronal dendritic complexity has been observed during chronic inflammation after traumatic brain injury (Ratliff et al., 2020; Witcher et al., 2021). Lipopolysaccharide (LPS) administration also decreases dendritic complexity in both the CA1 apical and basal subregions, while increasing proinflammatory cytokines in the hippocampus (Richwine et al., 2008). These findings confirm the link between neuroinflammation and neuronal structural plasticity. Collectively, our data suggest that dendritic complexity is strongly affected during the chronic phase of EAE, when neuroinflammation is pronounced (Lühder et al., 2013). However, we cannot exclude the possible involvement of the factors other than neuroinflammation, including defects in oligodendrocyte proliferation and glutamate-mediated excitotoxicity, which may interfere with aberrant structural changes in hippocampal neurons during EAE.

In contrast to dendritic complexity, we observed a more significant reduction in dendritic spine density in the early phase of EAE. Similarly, earlier research identified significant reductions in synaptic puncta within the CA1 subregion of EAE-affected mice during the early phase (Ziehn et al., 2010). Moreover, the number of dendritic spines was also found to be

markedly reduced in the hippocampi from post-mortem tissue from patients with MS (Dutta et al., 2011). In EAE, hippocampal synaptopathy is constitutively associated with pronounced microglial activation (Di Filippo et al., 2016; Mandolesi et al., 2015; Ziehn et al., 2010). Activated microglia can recognize and phagocytose unnecessary/nonfunctional synapses through complement-mediated pathways (Schafer et al., 2012; Stevens et al., 2007). Strikingly, these pathways may be aberrantly over-activated during the disease progression, resulting in severe spine reduction. However, the reasons for the prominent changes in spine density observed during the early phase, as opposed to the chronic phase (despite similar trends of decreased spine density in all regions during the chronic phase), remain unclear. Although the major proinflammatory cytokine expression did not reach statistical significance during the early phase, we observed a consistent tendency for reduced spine density in the chronic phase, which should not be overlooked. It is plausible that dominant factors, distinct from neuroinflammation, may regulate changes in spine density during the early phase, contributing to severe reductions despite the lack of statistical significance in major proinflammatory cytokine expression. Dendritic spines are minute structures that are plastic during both neuronal activity and at rest (Yuste & Bonhoeffer, 2001); even minute changes in the neuronal microenvironment and neuronal activation state can lead to changes in the structure of these spines (Lieshoff & Bischof, 2003). Thus, the changes in spine density observed during the course of EAE may be attributed to several factors, which should be further investigated.

Previously, we had observed transcript downregulation of IEGs (*Arc*, *FOS*, *Junb*, and *Egr1*) in the hippocampus during the chronic phase of EAE (Weerasinghe-Mudiyanselage et al., 2022b). Amongst these IEGs, *Arc*, the only activity-induced gene whose transcription is directly correlated with the inducing stimulus, is essential for synaptic plasticity and memory consolidation (Guzowski et al., 2001; Plath et al., 2006). Therefore, we examined the expression levels of ARC in the hippocampus during the chronic phase of EAE when dendritic complexity was most affected and found that ARC expression was significantly reduced in the EAE-affected hippocampi. Furthermore, immunostaining revealed reduced ARC immunoreactivity in the CA1 and DG subregions of the hippocampi of mice with EAE, coinciding with the structural changes in these subregions. Reduced IEG expression is often noted with reduced dendritic complexity and/or spine density in the hippocampus (Ka et al., 2016; Liu et al., 2016; Xie et al., 2013). Importantly, ARC directly interferes with dendritic and synaptic growth and reorganization by localized translation (Bramham et al., 2008; Korb & Finkbeiner, 2011). Therefore, the reduced levels of ARC in the hippocampus may help link the structural plasticity changes and altered hippocampus-related behavior observed in this animal model. Reduced ARC expression may result from diminished synaptic signaling or alterations in the turnover and/or translation of regulatory RNA-binding proteins or faster ARC degradation caused by proinflammatory effects (Rosi, 2011). Evidence for the latter is provided by the reduction in ARC expression in hippocampal neurons upon cytokine treatment.

Consistent with the structural changes and reduced ARC expression in the EAE animal model, primary cultures of hippocampal neurons demonstrated reduced dendritic complexity and ARC expression following treatment with proinflammatory cytokines. Furthermore, ERK phosphorylation was reduced following cytokine administration. The activity of IEGs, including ARC, is regulated via several signaling pathways, including the ERK/MAPK signaling pathway (Jiang et al., 2015; Ying et al., 2002). Therefore, in the present study, we investigated ERK phosphorylation following treatment with cytokines in primary cultures of hippocampal neurons as a plausible mechanism in ARC-mediated neuronal structural changes. ERK pathway-dependent expression of ARC in the hippocampus was reported in an experimental model of depression, while the alleviation of neuroinflammation restored the ERK and ARC expression together with reversal of depressive symptoms (Song et al., 2020). Thus, we propose that proinflammatory cytokines affect dendritic structural plasticity through the modulation of ARC expression, possibly through ERK signaling, leading to hippocampus-related behavioral changes. However, the possible involvement of other molecules regulated by the ERK/MAPK signaling pathway cannot be excluded, given its critical role in cell activation, proliferation, and differentiation, as well as neuroplasticity changes (Iroegbu et al., 2021; Newbern et al., 2011). Previous studies also suggest that various upstream signaling pathways, such as tropomyosin receptor kinase (Trk)A/nerve growth factor (Williams et al., 2006), TrkB/brain-derived neurotrophic factor (Yoshii & Constantine-Paton, 2010), neurotrophin-4 (NT-4), and TrkC/NT-3 (Gunn-Moore et al., 1997), can modulate ERK phosphorylation. Therefore, it is possible that one or more of these upstream signaling pathways may be affected in EAE hippocampi. To gain a comprehensive understanding of the mechanisms underlying the observed changes, further studies are needed to elucidate the intricate interplay of these signaling pathways in the context of EAE-induced alterations in structural plasticity.

In conclusion, our research demonstrated that EAE-affected mice exhibited anxiety-like behavior during both the early and chronic phases of the disease. Notably, we observed significant alterations in structural plasticity in the hippocampus during the chronic phase of EAE, coinciding with pronounced inflammation and initial declining trends in the acute phase. Our results suggest that cytokine-induced changes in structural plasticity may occur through inhibition of the ERK-ARC pathway (Figure 8). Nevertheless, it is important to note that these findings may be influenced by various factors, including the specific animal model, evaluation time points, and assessment methods. Thus, although this study provides new insights into hippocampal involvement in EAE, our results should be interpreted with caution. Future studies, including exploration in various MS animal models, are crucial to determine the overarching significance and accuracy of the structural alterations observed. In addition, further examination of the ERK-ARC pathway within this framework is essential, aiming to identify therapeutic strategies for hippocampus-related behavioral changes.

COMPETING INTERESTS

The authors declare that they have no competing interests.

AUTHORS' CONTRIBUTIONS

P.D.E.W-M. and C.M. designed the research. P.D.E.W-M., S.K., J.S.K., and C.M. performed the research. P.D.E.W-M., S.K., J.S.K., S.H.K., H.W., T.S., and C.M. acquired and analyzed the data. P.D.E.W-M. and C.M. wrote the original draft of the paper. P.D.E.W-M. and C.M. modified the manuscript. P.D.E.W-M., S.K., and C.M. wrote and edited the manuscript. All authors read and approved the final version of the manuscript.

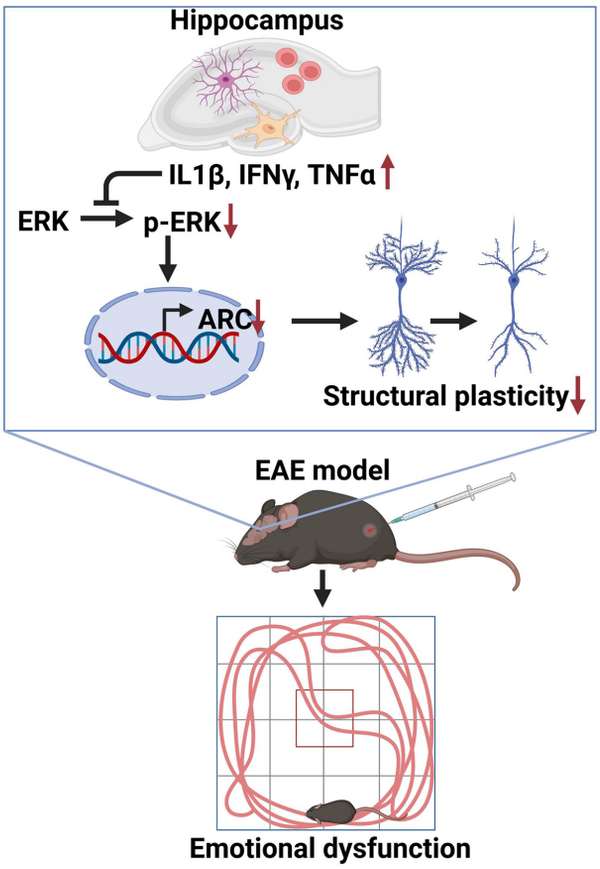

Figure 8 Schematic of potential link between altered structural plasticity in the hippocampus and hippocampal dysfunctions in EAE

Autoimmune neuroinflammation can interfere with the structural plasticity of hippocampal neurons, potentially through the ERK-ARC pathway. This modification may be associated with reported impairments in hippocampal functioning in EAE. ARC, activity-regulated cytoskeleton-associated protein; EAE, experimental autoimmune encephalomyelitis; ERK, extracellular signal-regulated kinases; Ifnγ, interferon gamma; Il1β, interleukin 1 beta; Tnfα, tumor necrosis factor alpha.

REFERENCES

Acharjee S, Nayani N, Tsutsui M, et al. 2013. Altered cognitive-emotional behavior in early experimental autoimmune encephalitis – cytokine and hormonal correlates. *Brain, Behavior, and Immunity*, **33**: 164−172.

Ang MJ, Kang S, Moon C. 2020. Melatonin alters neuronal architecture and increases cysteine-rich protein 1 signaling in the male mouse hippocampus. *Journal of Neuroscience Research*, **98**(11): 2333−2348.

Ang MJ, Lee S, Kim JC, et al. 2021. Behavioral tasks evaluating schizophrenia-like symptoms in animal models: a recent update. *Current Neuropharmacology*, **19**(5): 641−664.

Bannerman PG, Hahn A, Ramirez S, et al. 2005. Motor neuron pathology in experimental autoimmune encephalomyelitis: studies in THY1-YFP transgenic mice. *Brain*, **128**(Pt 8): 1877–1886.

Bellot A, Guivernau B, Tajes M, et al. 2014. The structure and function of actin cytoskeleton in mature glutamatergic dendritic spines. *Brain Research*, **1573**: 1−16.

Boldrini M, Fulmore CA, Tartt AN, et al. 2018. Human hippocampal neurogenesis persists throughout aging. *Cell Stem Cell*, **22**(4): 589−599.e5.

Bramham CR, Worley PF, Moore MJ, et al. 2008. The immediate early gene *Arc/Arg3.1*: regulation, mechanisms, and function. *Journal of Neuroscience*, **28**(46): 11760−11767.

Brochet B, Ruet A. 2019. Cognitive impairment in multiple sclerosis with regards to disease duration and clinical phenotypes. *Frontiers in Neurology*, **10**: 261.

Carassiti D, Altmann DR, Petrova N, et al. 2018. Neuronal loss, demyelination and volume change in the multiple sclerosis neocortex. *Neuropathology and Applied Neurobiology*, **44**(4): 377−390.

Centonze D, Muzio L, Rossi S, et al. 2009. Inflammation triggers synaptic alteration and degeneration in experimental autoimmune encephalomyelitis. *Journal of Neuroscience*, **29**(11): 3442−3452.

Centonze D, Muzio L, Rossi S, et al. 2010. The link between inflammation, synaptic transmission and neurodegeneration in multiple sclerosis. *Cell Death & Differentiation*, **17**(7): 1083−1091.

Colasanti A, Guo Q, Giannetti P, et al. 2016. Hippocampal neuroinflammation, functional connectivity, and depressive symptoms in multiple sclerosis. *Biological Psychiatry*, **80**(1): 62−72.

Di Filippo M, Chiasserini D, Gardoni F, et al. 2013. Effects of central and peripheral inflammation on hippocampal synaptic plasticity. *Neurobiology of Disease*, **52**: 229−236.

Di Filippo M, de Iure A, Durante V, et al. 2015. Synaptic plasticity and experimental autoimmune encephalomyelitis: implications for multiple sclerosis. *Brain Research*, **1621**: 205−213.

Di Filippo M, de Iure A, Giampà C, et al. 2016. Persistent activation of microglia and NADPH oxidase drive hippocampal dysfunction in experimental multiple sclerosis. *Scientific Reports*, **6**: 20926.

Di Filippo M, Portaccio E, Mancini A, et al. 2018. Multiple sclerosis and cognition: synaptic failure and network dysfunction. *Nature Reviews Neuroscience*, **19**(10): 599−609.

Di Filippo M, Sarchielli P, Picconi B, et al. 2008. Neuroinflammation and synaptic plasticity: theoretical basis for a novel, immune-centred, therapeutic approach to neurological disorders. *Trends in Pharmacological Sciences*, **29**(8): 402−412.

Dutta R, Chang AS, Doud MK, et al. 2011. Demyelination causes synaptic alterations in hippocampi from multiple sclerosis patients. *Annals of Neurology*, **69**(3): 445−454.

Dutra RC, Moreira ELG, Alberti TB, et al. 2013. Spatial reference memory deficits precede motor dysfunction in an experimental autoimmune encephalomyelitis model: the role of kallikrein-kinin system. *Brain, Behavior, and Immunity*, **33**: 90−101.

Furlan R, Cuomo C, Martino G. 2009. Animal models of multiple sclerosis. *In*: Gordon D, Scolding NJ. Neural Cell Transplantation. Totowa: Humana Press, 157–173.

Gentile A, Mori F, Bernardini S, et al. 2015. Role of amyloid-β CSF levels in cognitive deficit in MS. *Clinica Chimica Acta*, **449**: 23−30.

Geurts JJG, Bö L, Roosendaal SD, et al. 2007. Extensive hippocampal demyelination in multiple sclerosis. *Journal of Neuropathology & Experimental Neurology*, **66**(9): 819−827.

Gilmore JH, Fredrik Jarskog L, Vadlamudi S, et al. 2004. Prenatal infection and risk for schizophrenia: IL-1*β*, IL-6, and TNFα inhibit cortical neuron dendrite development. *Neuropsychopharmacology*, **29**(7): 1221−1229.

Gold SM, Kern KC, O'Connor MF, et al. 2010. Smaller cornu ammonis 2–3/dentate gyrus volumes and elevated cortisol in multiple sclerosis patients with depressive symptoms. *Biological Psychiatry*, **68**(6): 553−559.

Gunn-Moore FJ, Williams AG, Tavaré JM. 1997. Analysis of mitogen-activated protein kinase activation by naturally occurring splice variants of TrkC, the receptor for neurotrophin-3. *Biochemical Journal*, **322**(Pt 1): 193–198.

Guzowski JF, McNaughton BL, Barnes CA, et al. 2001. Imaging neural activity with temporal and cellular resolution using FISH. *Current Opinion in Neurobiology*, **11**(5): 579−584.

Haji N, Mandolesi G, Gentile A, et al. 2012. TNF-α-mediated anxiety in a mouse model of multiple sclerosis. *Experimental Neurology*, **237**(2):

296−303.

Hong S, Weerasinghe-Mudiyanselage PDE, Kang S, et al. 2023. Retinal transcriptome profiling identifies novel candidate genes associated with visual impairment in a mouse model of multiple sclerosis. *Animal Cells and Systems*, **27**(1): 219−233.

Iroegbu JD, Ijomone OK, Femi-Akinlosotu OM, et al. 2021. ERK/MAPK signalling in the developing brain: perturbations and consequences. *Neuroscience & Biobehavioral Reviews*, **131**: 792−805.

Ishizuka N, Weber J, Amaral DG. 1990. Organization of intrahippocampal projections originating from CA3 pyramidal cells in the rat. *Journal of Comparative Neurology*, **295**(4): 580−623.

Jiang Y, Liu YY, Zhu CS, et al. 2015. Minocycline enhances hippocampal memory, neuroplasticity and synapse-associated proteins in aged C57 BL/6 mice. *Neurobiology of Learning and Memory*, **121**: 20−29.

Ka M, Chopra DA, Dravid SM, et al. 2016. Essential roles for ARID1B in dendritic arborization and spine morphology of developing pyramidal neurons. *Journal of Neuroscience*, **36**(9): 2723−2742.

Kang S, Lee S, Kim J, et al. 2018. Chronic treatment with combined chemotherapeutic agents affects hippocampal micromorphometry and function in mice, independently of neuroinflammation. *Experimental Neurobiology*, **27**(5): 419−436.

Khorshid Ahmad T, Zhou T, AlTaweel K, et al. 2017. Experimental autoimmune encephalomyelitis (EAE)-induced elevated expression of the E1 isoform of methyl CpG binding protein 2 (MeCP2E1): implications in multiple sclerosis (MS)-induced neurological disability and associated myelin damage. *International Journal of Molecular Sciences*, **18**(6): 1254.

Kim B, Kim JS, Youn B, et al. 2023. Dopamine depletion alters neuroplasticity-related signaling in the rat hippocampus. *Animal Cells and Systems*, **27**(1): 436−446.

Kim B, Weerasinghe-Mudiyanselage PDE, Ang MJ, et al. 2022. Changes in the neuronal architecture of the hippocampus in a 6-hydroxydopamine-lesioned rat model of parkinson disease. *International Neurourology Journal*, **26**(S2): S94−105.

Kim DY, Hao JW, Liu RL, et al. 2012. Inflammation-mediated memory dysfunction and effects of a ketogenic diet in a murine model of multiple sclerosis. *PLoS One*, **7**(5): e35476.

Kim IJ, Beck HN, Lein PJ, et al. 2002. Interferon γ induces retrograde dendritic retraction and inhibits synapse formation. *Journal of Neuroscience*, **22**(11): 4530−4539.

Kim J, Ahn M, Choi Y, et al. 2019. Gene expression profile of olfactory transduction signaling in an animal model of human multiple sclerosis. *Experimental Neurobiology*, **28**(1): 74−84.

Ko W, Kim KW, Quang TH, et al. 2021. Cudraflavanone B isolated from the root bark of *Cudrania tricuspidata* alleviates lipopolysaccharide-induced inflammatory responses by downregulating NF-κB and ERK MAPK signaling pathways in RAW264.7 macrophages and BV2 microglia. *Inflammation*, **44**(1): 104−115.

Korb E, Finkbeiner S. 2011. Arc in synaptic plasticity: from gene to behavior. *Trends in Neurosciences*, **34**(11): 591−598.

Lee S, Yang M, Kim J, et al. 2016. Involvement of BDNF/ERK signaling in spontaneous recovery from trimethyltin-induced hippocampal neurotoxicity in mice. *Brain Research Bulletin*, **121**: 48−58.

Li XG, Somogyi P, Ylinen A, et al. 1994. The hippocampal CA3 network: an in vivo intracellular labeling study. *Journal of Comparative Neurology*, **339**(2): 181−208.

Lieshoff C, Bischof HJ. 2003. The dynamics of spine density changes. *Behavioural Brain Research*, **140**(1-2): 87−95.

Liu Y, Bian HJ, Xu SY, et al. 2020. Muscone ameliorates synaptic dysfunction and cognitive deficits in app/ps1 mice. *Journal of Alzheimer's Disease*, **76**(2): 491−504.

Liu ZH, Ding JJ, Yang QQ, et al. 2016. Early developmental bisphenol-a exposure sex-independently impairs spatial memory by remodeling hippocampal dendritic architecture and synaptic transmission in rats. *Scientific Reports*, **6**(1): 32492.

Livak KJ, Schmittgen TD. 2001. Analysis of relative gene expression data using real-time quantitative PCR and the 2(-Delta Delta C(T)) Method. *Methods (San Diego, Calif.)*, **25**(4): 402−408.

Lühder F, Gold R, Flügel A, et al. 2013. Brain-derived neurotrophic factor in neuroimmunology: lessons learned from multiple sclerosis patients and experimental autoimmune encephalomyelitis models. *Archivum Immunologiae et Therapiae Experimentalis*, **61**(2): 95−105.

Lyford GL, Yamagata K, Kaufmann WE, et al. 1995. Arc, a growth factor and activity-regulated gene, encodes a novel cytoskeleton-associated protein that is enriched in neuronal dendrites. *Neuron*, **14**(2): 433−445.

Ma QY, Geng Y, Wang HL, et al. 2019. High frequency repetitive transcranial magnetic stimulation alleviates cognitive impairment and modulates hippocampal synaptic structural plasticity in aged mice. *Frontiers in Aging Neuroscience*, **11**: 235.

Mandolesi G, Gentile A, Musella A, et al. 2015. Synaptopathy connects inflammation and neurodegeneration in multiple sclerosis. *Nature Reviews Neurology*, **11**(12): 711−724.

McEwen BS. 2004. Structural plasticity of the adult brain: how animal models help us understand brain changes in depression and systemic disorders related to depression. *Dialogues in Clinical Neuroscience*, **6**(2): 119−133.

Michailidou I, Willems JGP, Kooi EJ, et al. 2015. Complement C1q-C3-associated synaptic changes in multiple sclerosis hippocampus. *Annals of Neurology*, **77**(6): 1007−1026.

Moolman DL, Vitolo OV, Vonsattel JPG, et al. 2004. Dendrite and dendritic spine alterations in alzheimer models. *Journal of Neurocytology*, **33**(3): 377−387.

Morley BJ, Mervis RF. 2013. Dendritic spine alterations in the hippocampus and parietal cortex of alpha7 nicotinic acetylcholine receptor knockout mice. *Neuroscience*, **233**: 54−63.

Murphy LO, Smith S, Chen RH, et al. 2002. Molecular interpretation of ERK signal duration by immediate early gene products. *Nature Cell Biology*, **4**(8): 556−564.

Neumann H, Schweigreiter R, Yamashita T, et al. 2002. Tumor necrosis factor inhibits neurite outgrowth and branching of hippocampal neurons by a rho-dependent mechanism. *Journal of Neuroscience*, **22**(3): 854−862.

Newbern JM, Li XY, Shoemaker SE, et al. 2011. Specific functions for ERK/MAPK signaling during PNS development. *Neuron*, **69**(1): 91−105.

Nisticò R, Mango D, Mandolesi G, et al. 2013. Inflammation subverts hippocampal synaptic plasticity in experimental multiple sclerosis. *PLoS One*, **8**(1): e54666.

Novkovic T, Shchyglo O, Gold R, et al. 2015. Hippocampal function is compromised in an animal model of multiple sclerosis. *Neuroscience*, **309**: 100−112.

Pierson E, Simmons SB, Castelli L, et al. 2012. Mechanisms regulating regional localization of inflammation during CNS autoimmunity. *Immunological Reviews*, **248**(1): 205−215.

Planche V, Panatier A, Hiba B, et al. 2017. Selective dentate gyrus disruption causes memory impairment at the early stage of experimental multiple sclerosis. *Brain, Behavior, and Immunity*, **60**: 240−254.

Plath N, Ohana O, Dammermann B, et al. 2006. Arc/Arg3.1 is essential for the consolidation of synaptic plasticity and memories. *Neuron*, **52**(3): 437−444.

Procaccini C, De Rosa V, Pucino V, et al. 2015. Animal models of multiple sclerosis. *European Journal of Pharmacology*, **759**: 182−191.

Ratliff WA, Delic V, Pick CG, et al. 2020. Dendritic arbor complexity and spine density changes after repetitive mild traumatic brain injury and neuroprotective treatments. *Brain Research*, **1746**: 147019.

Richwine AF, Parkin AO, Buchanan JB, et al. 2008. Architectural changes to CA1 pyramidal neurons in adult and aged mice after peripheral immune stimulation. *Psychoneuroendocrinology*, **33**(10): 1369−1377.

Rizzo FR, Musella A, De Vito F, et al. 2018. Tumor necrosis factor and interleukin-1*β* modulate synaptic plasticity during neuroinflammation. *Neural Plasticity*, **2018**: 8430123.

Rocca MA, Barkhof F, De Luca J, et al. 2018. The hippocampus in multiple sclerosis. *The Lancet Neurology*, **17**(10): 918−926.

Rosi S. 2011. Neuroinflammation and the plasticity-related immediate-early gene *Arc*. *Brain, Behavior, and Immunity*, **25 Suppl 1** (S1): S39–S49.

Rossi S, Furlan R, De Chiara V, et al. 2009. Exercise attenuates the clinical, synaptic and dendritic abnormalities of experimental autoimmune encephalomyelitis. *Neurobiology of Disease*, **36**(1): 51−59.

Rossi S, Motta C, Studer V, et al. 2014. Interleukin-1β causes excitotoxic neurodegeneration and multiple sclerosis disease progression by activating the apoptotic protein p53. *Molecular Neurodegeneration*, **9**: 56.

Rouleau I, Dagenais E, Tremblay A, et al. 2018. Prospective memory impairment in multiple sclerosis: a review. *The Clinical Neuropsychologist*, **32**(5): 922−936.

Schafer DP, Lehrman EK, Kautzman AG, et al. 2012. Microglia sculpt postnatal neural circuits in an activity and complement-dependent manner. *Neuron*, **74**(4): 691−705.

Seibenhener ML, Wooten MC. 2015. Use of the open field maze to measure locomotor and anxiety-like behavior in mice. *Journal of Visualized Experiments*, (96): e52434.

Sholl DA. 1953. Dendritic organization in the neurons of the visual and motor cortices of the cat. *Journal of Anatomy*, **87**(4): 387−406.

Sicotte NL, Kern KC, Giesser BS, et al. 2008. Regional hippocampal atrophy in multiple sclerosis. *Brain*, **131**(Pt 4): 1134–1141.

Sloane E, Ledeboer A, Seibert W, et al. 2009. Anti-inflammatory cytokine gene therapy decreases sensory and motor dysfunction in experimental multiple sclerosis: MOG-EAE behavioral and anatomical symptom treatment with cytokine gene therapy. *Brain, Behavior, and Immunity*, **23**(1): 92−100.

Son Y, Kang S, Kim J, et al. 2016. Possible involvement of hippocampal immediate-early genes in contextual fear memory deficit induced by cranial irradiation. *Neurobiology of Learning and Memory*, **133**: 19−29.

Song ZJ, Shen FM, Zhang ZR, et al. 2020. Calpain inhibition ameliorates depression-like behaviors by reducing inflammation and promoting synaptic protein expression in the hippocampus. *Neuropharmacology*, **174**: 108175.

Stampanoni Bassi M, Garofalo S, Marfia GA, et al. 2017. Amyloid-β homeostasis bridges inflammation, synaptic plasticity deficits and cognitive dysfunction in multiple sclerosis. *Frontiers in Molecular Neuroscience*, **10**: 390.

Stampanoni Bassi M, Iezzi E, Centonze D. 2022. Multiple sclerosis: inflammation, autoimmunity and plasticity. *Handbook of Clinical Neurology*, **184**: 457−470.

Stampanoni Bassi M, Iezzi E, Mori F, et al. 2019. Interleukin-6 disrupts synaptic plasticity and impairs tissue damage compensation in multiple sclerosis. *Neurorehabilitation and Neural Repair*, **33**(10): 825−835.

Stefanova NA, Maksimova KY, Kiseleva E, et al. 2015. Melatonin attenuates impairments of structural hippocampal neuroplasticity in OXYS rats during active progression of Alzheimer's disease-like pathology. *Journal of Pineal Research*, **59**(2): 163−177.

Stevens B, Allen NJ, Vazquez LE, et al. 2007. The classical complement cascade mediates CNS synapse elimination. *Cell*, **131**(6): 1164−1178.

Tsai ST, Chen SY, Lin SZ, et al. 2020. Rostral intralaminar thalamic deep brain stimulation ameliorates memory deficits and dendritic regression in β-amyloid-infused rats. *Brain Structure and Function*, **225**(2): 751−761.

Tu JL, Zhao CB, Vollmer T, et al. 2009. APOE 4 polymorphism results in early cognitive deficits in an EAE model. *Biochemical and Biophysical Research Communications*, **384**(4): 466−470.

Wada M, Ang MJ, Weerasinghe-Mudiyanselage PDE, et al. 2021. Behavioral characterization in MPTP/p mouse model of Parkinson's disease. *Journal of Integrative Neuroscience*, **20**(2): 307−320.

Weerasinghe-Mudiyanselage PDE, Ang MJ, Kang S, et al. 2022a. Structural plasticity of the hippocampus in neurodegenerative diseases. *International Journal of Molecular Sciences*, **23**(6): 3349.

Weerasinghe-Mudiyanselage PDE, Ang MJ, Wada M, et al. 2021a. Acute MPTP treatment impairs dendritic spine density in the mouse hippocampus. *Brain Sciences*, **11**(7): 833.

Weerasinghe-Mudiyanselage PDE, Kang S, Kim JS, et al. 2022b. Transcriptome profiling in the hippocampi of mice with experimental autoimmune encephalomyelitis. *International Journal of Molecular Sciences*, **23**(23): 14829.

Weerasinghe-Mudiyanselage PDE, Kang S, Kim JS, et al. 2023. Therapeutic approaches to non-motor symptoms of parkinson's disease: a current update on preclinical evidence. *Current Neuropharmacology*, **21**(3): 560−577.

Weerasinghe-Mudiyanselage PDE, Kim J, Choi Y, et al. 2021b. Ninjurin-1: a biomarker for reflecting the process of neuroinflammation after spinal cord injury. *Neural Regeneration Research*, **16**(7): 1331−1335.

Weerasinghe-Mudiyanselage PDE, Kim JS, Shin T, et al. 2024. Understanding the spectrum of non-motor symptoms in multiple sclerosis: insights from animal models. *Neural Regeneration Research*, **19**(1): 84−91.

Williams BJ, Bimonte-Nelson HA, Granholm-Bentley AC. 2006. Erk-mediated NGF signaling in the rat septo-hippocampal pathway diminishes with age. *Psychopharmacology*, **188**(4): 605−618.

Witcher KG, Bray CE, Chunchai T, et al. 2021. Traumatic brain injury causes chronic cortical inflammation and neuronal dysfunction mediated by microglia. *Journal of Neuroscience*, **41**(7): 1597−1616.

Xie L, Korkmaz KS, Braun K, et al. 2013. Early life stress-induced histone acetylations correlate with activation of the synaptic plasticity genes Arc and egr1 in the mouse hippocampus. *Journal of Neurochemistry*, **125**(3): 457−464.

Yang MYN, Kim JS, Song MS, et al. 2010. Cyclophosphamide impairs hippocampus-dependent learning and memory in adult mice: possible involvement of hippocampal neurogenesis in chemotherapy-induced memory deficits. *Neurobiology of Learning and Memory*, **93**(4): 487−494.

Ying SW, Futter M, Rosenblum K, et al. 2002. Brain-derived neurotrophic factor induces long-term potentiation in intact adult hippocampus: requirement for ERK activation coupled to CREB and upregulation of *Arc* synthesis. *Journal of Neuroscience*, **22**(5): 1532−1540.

Yoshii A, Constantine-Paton M. 2010. Postsynaptic BDNF-TrkB signaling in synapse maturation, plasticity, and disease. *Developmental Neurobiology*, **70**(5): 304−322.

Yuste R, Bonhoeffer T. 2001. Morphological changes in dendritic spines associated with long-term synaptic plasticity. *Annual Review of Neuroscience*, **24**(1): 1071−1089.

Zheng FL, Li YX, Zhuo ZZ, et al. 2022. Structural and functional hippocampal alterations in multiple sclerosis and neuromyelitis optica spectrum disorder. *Multiple Sclerosis Journal*, **28**(5): 707−717.

Ziehn MO, Avedisian AA, Tiwari-Woodruff S, et al. 2010. Hippocampal CA1 atrophy and synaptic loss during experimental autoimmune encephalomyelitis, EAE. *Laboratory Investigation*, **90**(5): 774−786.

Zorzella-Pezavento SFG, Chiuso-Minicucci F, França TGD, et al. 2013. Persistent inflammation in the CNS during chronic EAE despite local absence of IL-17 production. *Mediators of Inflammation*, **2013**: 519627.